European Journal of Pharmaceutics and Biopharmaceutics 158 (2021) 294–312

Contents lists available at ScienceDirect

European Journal of Pharmaceutics and Biopharmaceutics

journal homepage: www.elsevier.com/locate/ejpb

Versatility of hydrogel-forming microneedles in *in vitro* transdermal delivery of tuberculosis drugs

Qonita Kurnia Anjani [a], Andi Dian Permana [b], Álvaro Cárcamo-Martínez [a], Juan Domínguez-Robles [a], Ismaiel A. Tekko [a,c], Eneko Larrañeta [a], Lalit K. Vora [a], Delly Ramadon [a,d], Ryan F. Donnelly [a,*]

[a] School of Pharmacy, Queen's University Belfast, Medical Biology Centre, 97 Lisburn Road, Belfast BT9 7BL, UK
[b] Department of Pharmaceutics, Faculty of Pharmacy, Hasanuddin University, Makassar, Indonesia
[c] Department of Pharmaceutics and Pharmaceutical Technology, Faculty of Pharmacy, Aleppo University, Aleppo, Syria
[d] Faculty of Pharmacy, University of Indonesia, West Java, Indonesia

ARTICLE INFO

Keywords:
Tuberculosis drug regime
Hydrogel-forming microneedle array
Drug reservoir optimisation
Permeation studies

ABSTRACT

Current therapy of tuberculosis (TB) has several limitations, such as risk of liver injury and intestinal dysbiosis due to frequent oral administration of antibiotics. Transdermal administration could be used to improve antibiotic delivery for treatment of *Mycobacterium tuberculosis* infection. Therefore, we developed a novel approach, using hydrogel-forming microneedle (MN) arrays to transdermally deliver TB drugs, namely rifampicin, isoniazid, pyrazinamide and ethambutol, which have different physicochemical properties. These drugs were individually prepared into three types of drug reservoirs, including lyophilised tablets, directly compressed tablets and poly(ethylene glycol) tablets. Formulations of each drug reservoir type were optimised to achieve a rapidly dissolving tablet, and further integrated with hydrogel-forming MN arrays for *in vitro* permeation studies. Three types of hydrogel formulation were manufactured using different type of polymers and crosslinking processes. These MN arrays were then evaluated in terms of swelling ability, morphology and physical properties. Results of solute diffusion studies showed that drug permeation across the swollen hydrogel membrane was affected mostly by physiochemical properties and functional groups of each drug. In the *in vitro* studies, the amount of permeated drug through the hydrogel-forming MN arrays across the dermatomed neonatal porcine skin was affected by the drug solubility and reservoir design. The highest permeation of rifampicin (3.64 mg) and ethambutol (46.99 mg) were achieved using MN arrays combined with the poly(ethylene glycol) tablets and directly compressed tablet, respectively. For isoniazid and pyrazinamide, the highest drug permeation was attained using lyophilised reservoir with the amount of drug delivered approximately 58.45 mg and 20.08 mg, respectively. These equate to transdermal delivery of approximately 75% (rifampicin), 79% (isoniazid), 20% (pyrazinamide) and 47% (ethambutol) of the drugs loaded into the reservoirs on average. Importantly, the results of this work have demonstrated the versatility of hydrogel formulations to deliver a TB drug regime using MN arrays. Accordingly, this is a promising approach to deliver high dose of TB drugs.

1. Introduction

Tuberculosis (TB) is an airborne infectious disease caused by *Mycobacterium tuberculosis* [1]. The World Health Organization (WHO) reported that in 2019, about one-quarter people in the world have been infected by this TB microorganism [2]. These figures include both asymptomatic and active TB cases, as the progression of the latent TB infection. Respiratory problems are one of the most common symptoms that appear in active TB cases as the microorganism lives dormantly in the lungs before the symptomatic disease starts [3]. Currently, the first-line treatment option for TB consists of a multi-drug regimen, particularly rifampicin (RIF), isoniazid (INH), pyrazinamide (PYR) and ethambutol (ETH) [2,4–6]. Oral administration is popular in TB treatment due to its convenience affordability and low cost in terms of patient

* Corresponding author at: Chair in Pharmaceutical Technology, School of Pharmacy, Queen's University Belfast, Medical Biology Centre, 97 Lisburn Road, Belfast BT9 7BL, Northern Ireland, UK.
E-mail address: r.donnelly@qub.ac.uk (R.F. Donnelly).

https://doi.org/10.1016/j.ejpb.2020.12.003
Received 3 August 2020; Received in revised form 2 December 2020; Accepted 6 December 2020
Available online 9 December 2020

experience. However, using this route, patients need to take high doses for prolonged periods of time [7,8]. Moreover, the oral route has limitations and can result in chronic side effects as a result of frequent administration [9,10]. On the other hand, the parenteral route and direct pulmonary delivery can reach the target site by escaping hepatic first-pass metabolism. As a result, these routes can reach the highest bioavailability compared to the other routes [7]. Regardless, drug delivery by parenteral routes requires healthcare skill and often results in poor patient compliance [11]. In addition, drug delivered *via* the pulmonary route can be quickly removed from the lungs and the duration of drug action can be shortened due to a range of mechanisms of lung clearance [12].

Transdermal drug delivery (TDD) may circumvent many of the above-mentioned issues, while offering a more convenient treatment approach for patients. Nowadays, TDD is focused on *stratum corneum* modification, as the main barrier of this administration route, rather than altering the molecular properties of active substances [13]. According to the list of transdermal products that have been marketed, the limitation of transdermal patches is that they tend to be used for delivery of high potent and small-dose drugs [14]. Therefore, transdermal delivery of high-dose drugs, as required for TB treatment, is quite challenging. Conventional patches are not able to load and deliver the required dose to treat TB bacteria infection. Accordingly, an alternative and innovative approach to TDD is urgently required to address these challenges. To date, there have been no published studies investigating transdermal delivery of TB drugs. Thus, this study aimed to develop, for the first time, a TDD platform for delivery of RIF, INH, PYR and ETH to improve TB treatment.

In order to deliver high-dose drugs required in TB regime across the *stratum corneum* to reach the dermal microcirculation, microneedle (MN) array technology could be an option to improve drug permeation. MN delivery systems have the ability to penetrate into the deeper layers of skin and can easily pass through the *stratum corneum* barrier [15–17]. MN arrays are minimally invasive devices that consist of a series of microscopic needles (height ranging from 50 to 900 μm) attached to a base support [18]. They can penetrate to the dermis, but are still short and narrow enough to avoid reaching the dermal nerves and blood vessels [19]. Moreover, the MN array offers possible uniformity of transdermal dosing, as it completely bypasses the skin barrier, potentially overcoming individual skin thickness and variability problems [20].

Hydrogel-forming MN arrays are one type of MN which are prepared through a crosslinking process from an aqueous mixture of polymers [21]. Composed of micron-scale needles arranged on a baseplate, they are devoid of any drug. Instead, the drug is contained within a reservoir attached to the upper side of the base plate. Following the insertion into the skin, they imbibe interstitial fluid from the skin tissue below. This allows diffusion of the drug from the attached reservoir layer to the dermal microcirculation, ultimately reaching the systemic circulation [22]. Several studies reported the capability of hydrogel-forming MN arrays to deliver a variety of molecules effectively, such as hydrophilic, hydrophobic, high molecular and high dose substances [18,22–25]. Hydrogel-forming MN arrays offer advantages over other MN types, such as dissolving MN arrays, in that they can be removed from the skin intact and, thus, do not result in polymer deposition in the skin. They are also not limited to delivery of drugs contained within the needles themselves [23].

In the present work, we developed different types of hydrogel system and investigated the permeation of TB drugs through those hydrogel formulations to select the potential materials for fabricating the hydrogel-forming MN arrays. Furthermore, in order to achieve a high permeation of TB drugs, a suitable formulation of drug reservoir is also important to be considered. The concept of rapidly dissolving tablets, as the reservoir, become the key feature to develop this system considering the limited amount of aqueous medium provided by swollen hydrogel-forming MN arrays [18]. Several approaches have been discussed to develop drug reservoirs with rapid dissolution characteristics, including direct compressing, lyophilisation and solid dispersion methods [26–28]. Therefore, the aforementioned methods were used and optimised in the present work to tailor a reservoir expected to release drug molecules immediately through swollen hydrogel-forming MN arrays after insertion into skin [23]. With respect to the use of hydrogel-forming MN arrays, this technology has been investigated for delivery of various types of drugs, including ibuprofen-sodium, olanzapine, ovalbumin and metformin. Furthermore, this delivery platform has also been coupled with several drug-containing reservoirs, such as lyophilised and liquid reservoirs. It is not surprising, however, in the previous published sources mentioned above, each drug was delivered using one type of hydrogel-forming MN arrays. To the best of our knowledge, there were not studies which performed the versatility of hydrogel-forming MN arrays for delivery of drugs with different physicochemical characteristics. The aim of this study was, therefore, to investigate the versatility of hydrogel type and, for the first time, effect of the reservoir design on the delivery of TB drugs with different molecular properties. This study can also provide insights into the range of different drug compounds that could potentially be delivered using hydrogel-forming MN arrays.

Table 1
Hydrogel film formulation and crosslinking conditioning.

Formula	Composition in water (%w/w)	Temperature (°C)	Crosslinking time
H1	20% Gantrez® S-97, 7.5% PEG 10,000, 3% Na_2CO_3	80	24 h
H2	15% PVA, 10% PVP, 1.5% citric acid	130	3 h
H3	15% PVA, 10% PVP, 1.5% citric acid	130	40 min

2. Material and methods

2.1. Materials

Rifampicin (molecular biology reagent), isonicotinic acid hydrazide (purity, ≥98%), pyrazinamide (purity, 98%), ethambutol dihydrochloride were purchased from Alfa Aesar (Lancashire, UK). Gantrez® S-97, a copolymer of methylvinylether and maleic acid (PMVE/MA) with molecular weight of 1,500 kDa and poly (vinyl pyrrolidone) (PVP) with molecular weight of 58 kDa were provided by Ashland, Kidderminster, UK. Crospovidone, (Kollidon® CL-SF) was purchased from BASF (Ludwigshafen, Germany). Phenetyl isocyanate (PEIC) was purchased from Tokyo Chemical Industry (Oxford, UK). Sodium starch glycolate (SSG) was purchased from DFE Pharma, Klever Strasse, Germany. Ultrapure water was obtained from a water purification system (Elga PURELAB DV 25, Veolia Water Systems, Dublin, Ireland). All other chemicals and materials were of analytical grade and purchased from Sigma-Aldrich (Dorset, UK) or Fisher Scientific (Loughborough, UK).

2.2. Fabrication of hydrogel films

Stock solutions of Gantrez® S-97 (40% w/w), PVA (25% w/w) and PVP (40% w/w) were prepared using deionised water. Each of Gantrez® S-97 and PVA-based hydrogel films were then prepared as previously described [18,29]. Hydrogel film formulations are shown in Table 1 and the preparation process is illustrated in Fig. 1. Each aqueous blend was centrifuged (Eppendorf® 5804 series centrifuge, Fisher Scientific, Loughborough, UK) at 5,000 rpm for 15 min to remove air bubbles. A 30 g aliquot of each blend was carefully poured into separate (100 mm × 100 mm) flat Perspex base plate lined with a siliconised-release liner on the surface and secured with stainless-steel clamps. The blends were then dried at room temperature for 48 h. The dried films were then removed from the moulds and cut into smaller pieces (10 mm × 10 mm).

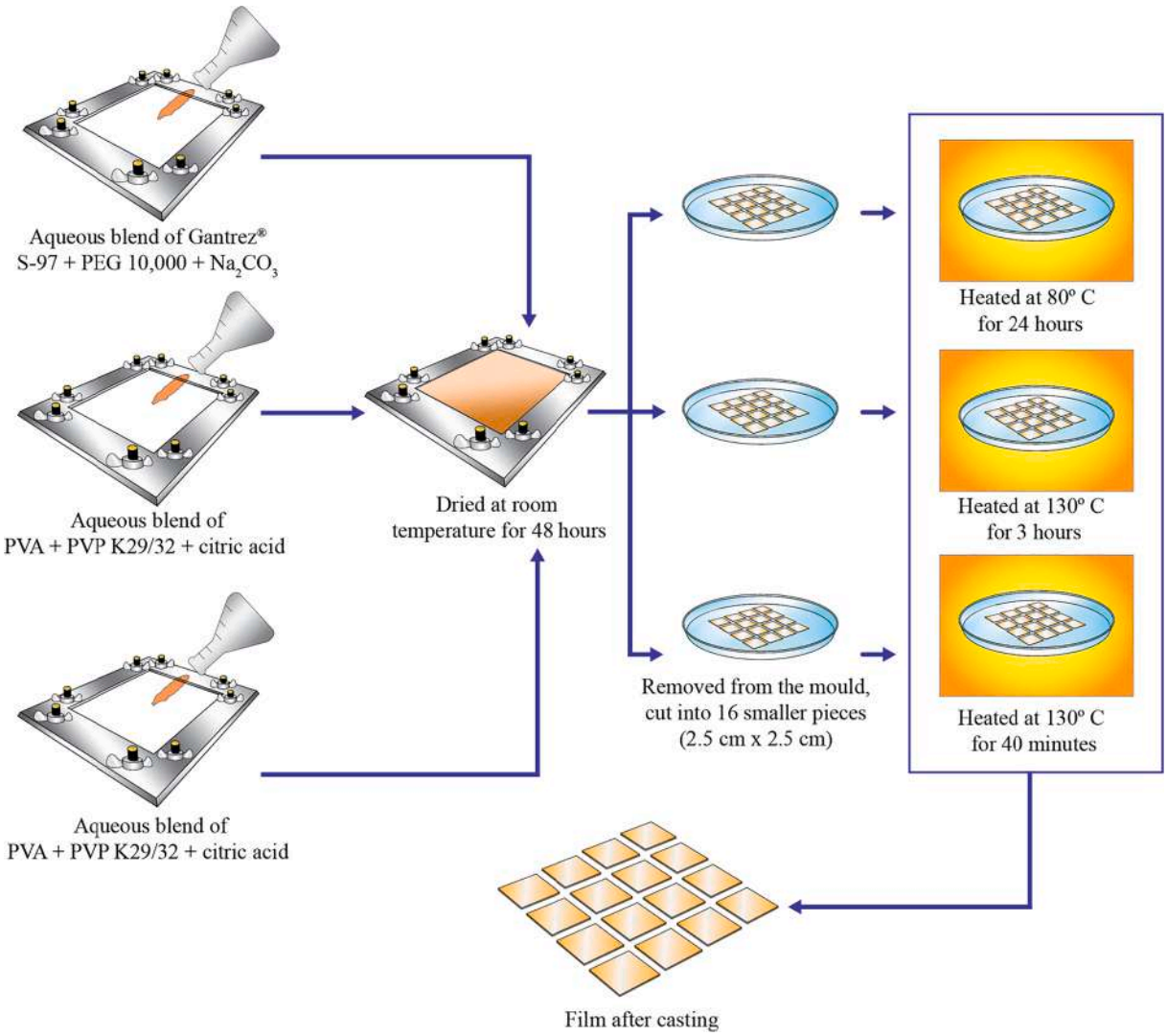

Fig. 1. Schematic representation of hydrogel film preparation and crosslinking.

Following this, H1 was crosslinked at 80 °C for 24 h [18]. In the case of PVA, films were heated for different times for crosslinking, 130 °C for 3 h (H2) and at 130 °C for 40 min (H3) to induce chemical crosslinking (esterification reaction) [30–32]. Once films were removed from the oven, they were ready to be used for permeation studies.

2.3. Swelling studies of hydrogel films

Swelling studies were carried out using a method previously described [18]. Approximately 100 mm^2 of the films were weighed in the dry state and recorded as m_0, then immersed into PBS pH 7.4 and removed at specific time points. Films were dried with filter paper to remove excess of PBS on the surface and weighed as m_t. Percentage of swelling was calculated using Eq. (1) [30,33,34].

$$\%\ Swelling = \frac{(m_t - m_0)}{m_0} \times 100\% \quad (1)$$

where, m_t is the mass of film at 24 h and m_0 is the initial mass of film.

The percentage equilibrium water content (EWC) reflects the maximum amount of water that can be absorbed by a hydrogel. In order to calculate EWC percentage, the hydrogel samples at equilibrium, defined as the swelling percentage at which there is no marked change in hydrogel mass, were weighed and recorded as m_s. EWC percentage was obtained using Eq. (2) [35,36].

$$\%EWC = \frac{(m_s - m_0)}{m_s} \times 100\% \quad (2)$$

where, m_s is the mass of swollen film at equilibrium and m_0 is the initial mass of film.

2.4. Morphology of hydrogel films

Hydrogel film visualization was achieved by SEM with a Quanta FEG 250 microscope (FEI, Hillsboro OR, USA) at an acceleration voltage of 5–20 kV under high chamber pressure (8×10^{-5} mbar) with standard SEM carbon tape as background. For sample preparation, films were immersed in PBS pH 7.4 for 24 h at room temperature and then pre-frozen at −80 °C for 3 h to prepare samples for the lyophilisation process. Samples were lyophilised in a freeze drier (Virtis™ Advantage XL-70, SP Scientific, Warminster PA, USA) for 24 h, following a cycle of primary drying for 13 h at a shelf temperature starting from −40 °C, secondary drying for 11 h at 25 °C and vacuum pressure of 50mTorr. After that, dried samples were fixed onto an aluminium stub and sputter coated with pure gold.

2.5. Solute diffusion studies

Side-by-side diffusion cells (Permergear, Hellertown PA, USA) were

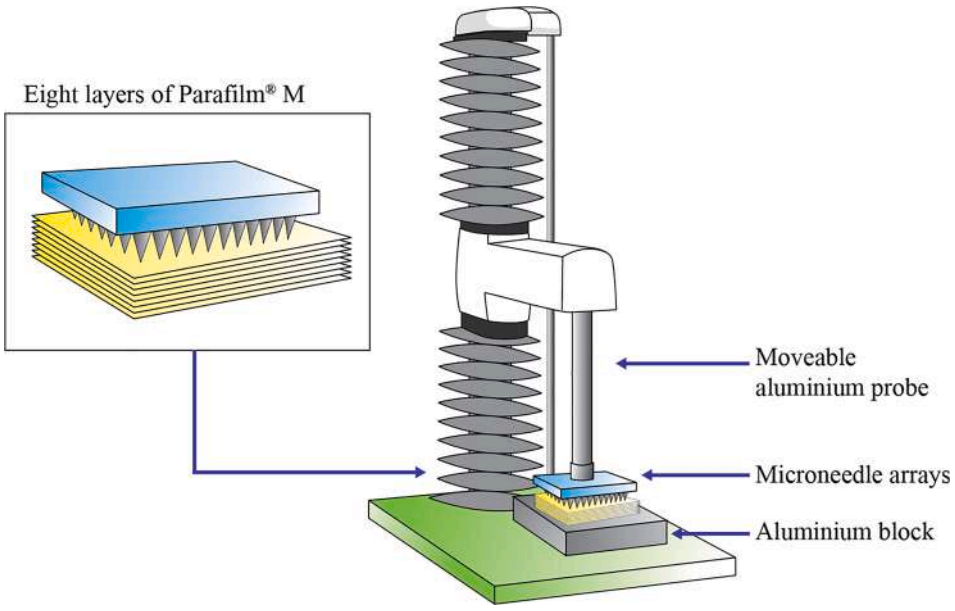

Fig. 2. Texture Analyser setup for determining compression resistance of microneedle arrays.

used to determine drug permeation across the swollen hydrogel films. Firstly, films were pre-equilibrated in PBS pH 7.4 for 24 h, and then cut into a round shape with a diameter of 9 mm^2 to cover the cavity between the donor and receptor compartments. Each membrane was clamped between the two-half compartments and the interface was covered by Parafilm® M to prevent leakage and evaporation. A 3 mL volume of 1 mg/mL solution for each drug was added to the donor compartment. PBS pH 7.4 was added to the receptor compartment in the case of INH, PYR and ETH. To achieve sink conditions and maintain drug stability, PBS pH 7.4 containing sodium lauryl sulphate (1% w/v) and ascorbic acid (0.1% w/v) was used in the specific case of RIF. An aliquot (3 mL) from the receptor solution was taken at predetermined time intervals and replaced with the same amount of fresh medium. All samples were then analysed using a validated of high-performance liquid chromatography (HPLC) method, as described in Section 2.13.

2.6. Fabrication of hydrogel-forming MN arrays

Hydrogel-forming MN arrays were prepared from the same stock solutions outlined in Section 2.2. Initially, 500 mg of an aqueous blend of each formulation were carefully poured into 11 × 11 pre-formed silicone MN moulds (conical shape, 600 μm height, 300 μm width at the base, and 300 μm interspacing). Following this, the moulds were centrifuged (Eppendorf® 5804 series centrifuge, Fisher Scientific, Loughborough, UK) at 5,000 rpm for 15 min and then dried at room temperature for 48 h. The cast MN arrays were removed from the mould and then heated at 80 °C or 130 °C for 24 h, 3 h and 40 min, as shown in Table 1 for the corresponding films.

2.7. Mechanical resistance and skin insertion study

Resistance to compression of the MN arrays were evaluated using a TA-TX2 Texture Analyser (TA) (Stable Microsystems, Haslmere, UK) in compression mode, as previously reported [18,21,37] (see Fig. 2). The height of MN arrays before and after testing was measured and recorded using a digital light microscope (Leica EZ4 D, Leica Microsystems, Milton Keynes, UK). The percentage MN height reduction was then calculated using Eq. (3).

$$Height\ \ reduction(\%) = \frac{H_a - H_b}{H_a} \times 100\% \quad (3)$$

where Ha is the height before compression and Hb is the height after compression.

MN arrays' insertion properties were studied using TA and the validated skin model, Parafilm® M [38]. Eight sheets of Parafilm® M were arranged into an eight-layer film (approximately 1 mm thickness). Next, MN arrays were attached to a cuboidal probe (cross-sectional area 1 cm^2) using double-sided adhesive tape. The probe moved downwards at a speed of 1.19 mm/s until a pre-set force, 32 N, was reached. The force was then held for 30 s and the inserted MN arrays were immediately removed and then Parafilm® M sheets unfolded, and the number of holes produced in each layer using the light microscope. The percentage of holes in each layer relative to the number of MN on the array was determined using Eq. (4).

$$Holes\ in\ Parafilm^{\circledR}M\ (\%) = \frac{number\ of\ holes\ observed}{number\ of\ MN\ in\ an\ array} \times 100 \quad (4)$$

In addition, the insertion of MN arrays into full-thickness neonatal porcine skin was examined using an optical coherence tomography (OCT) microscope (EX1301 VivoSight®, Michelson Diagnostics Ltd, Kent, UK). ImageJ® (National Institutes of Health, Bethesda MD, USA) was used to measure the height of needles inserted [15,38].

2.8. Preparation of lyophilised reservoirs

Sucrose, mannitol, glycine and trehalose were all screened as bulking agent for the preparation of reservoirs. Lyophilised (LYO) reservoir formulations were optimised using three-factor and two-level central composite designs (CCD) using Design Expert Software version 12 (State-ease, Minneapolis MN, USA). The experimental design for LYO reservoir optimisations is displayed in Table S1 for RIF, and Table S2 (supplementary information) for INH/PYR. In the optimisation process, drug, gelatin and bulking agent concentration were used as variable factors. Dissolution time and hardness were recorded as the responses.

All powder blend components were homogenised using a Vortex™ (Fisons Scientific Equipment, Loughborough, Leicestershire, UK) for 1 min and then an appropriate volume of deionised water was added to the mixture to complete the required total mass of the reservoir. The aqueous mixture was once again homogenised using a Vortex™ for 1 min and sonicated at 37 °C for 60 min. Approximately 150 mg of each mixture was cast into a customised open-ended cylindrical mould (diameter of 8 mm and depth of 4 mm). Then, the cast mixtures were

Table 2
Formulation of PEG reservoir.

Components	Composition (%w/w)		
	P1	P2	P3
PEG 200	75	50	25
PEG 6,000	25	50	75

frozen at −80 °C for 3 h to prepare the samples for the lyophilisation process. These formulations were lyophilised in the freeze drier for 24 h, following a cycle of −40 °C for primary drying and 25 °C for secondary drying with a pressure of 50 m Torr.

ETH LYO reservoirs were formulated by varying gelatin concentration and the total reservoir mass, due to ETH solubility properties. Firstly, gelatin was dissolved in an appropriate amount of deionised water. Afterwards, ETH was dispersed in the gelatin solution and the aqueous blend homogenised using a Vortex™ for 1 min. The mixture was then cast and lyophilised using the method previously described.

2.9. Preparation of directly compressed tablet as reservoirs

Directly compressed tablets (DCT) reservoirs were prepared using a manual hydraulic press (Specac® Atlas, Specac Ltd, Kent, UK). Prior to compression, each drug and disintegrating agent were weighed and mixed using a Vortex™ for 1 min. Approximately 150 mg of a powder mixture from each formulation was accurately weighed and then placed into the tablet die manually. A 5 tonnes compression pressure was applied for each formulation of DCT reservoirs. The pressure was held for 1 min and the formed tablet was then removed from the machine. A variety of disintegrating was screened in this work, namely sorbitol, mannitol, crospovidone and sodium starch glycolate (SSG). DCT formulations were optimised using two-level and two response factors of CCD, recording dissolution time and hardness as the two responses. In the specific case of ETH, based on preliminary studies, DCTs were formulated without any excipients. The experimental design optimisation for the DCT formulation of RIF and INH/PYR is shown in Table S3 and Table S4 (supplementary information), respectively.

2.10. Preparation of poly(ethylene glycol) solid reservoirs

The reservoir formulations were prepared using a solid dispersion (SD) method with slight modifications [39,40]. Poly(ethylene glycol) (PEG) reservoirs were fabricated using PEG 6000 as a solid base and PEG 200 as a liquid cosolvent. The formulation of a drug-containing reservoir was prepared by varying the proportion of both PEG 200 and 6000, as detailed in Table 2. The mixture of drug and PEG was prepared to obtain final reservoirs containing 11 mg of each TB drug. Initially, a mixture was prepared by dissolving each drug in PEG 200 in a glass vial and then mixed using a Vortex™ for 1 min. Afterwards, a weighed amount of PEG 6,000 was dispersed into the solution and then transferred to an oven at 70 °C for 30 min to obtain a homogeneous mixture. The reservoirs were formed by pouring 250 mg of the mixture into 10 mm × 10 mm square silicone moulds. Afterwards, the silicone mould was refrigerated at −20 °C for 15 min. The reservoirs were ready to be removed after completed solidification.

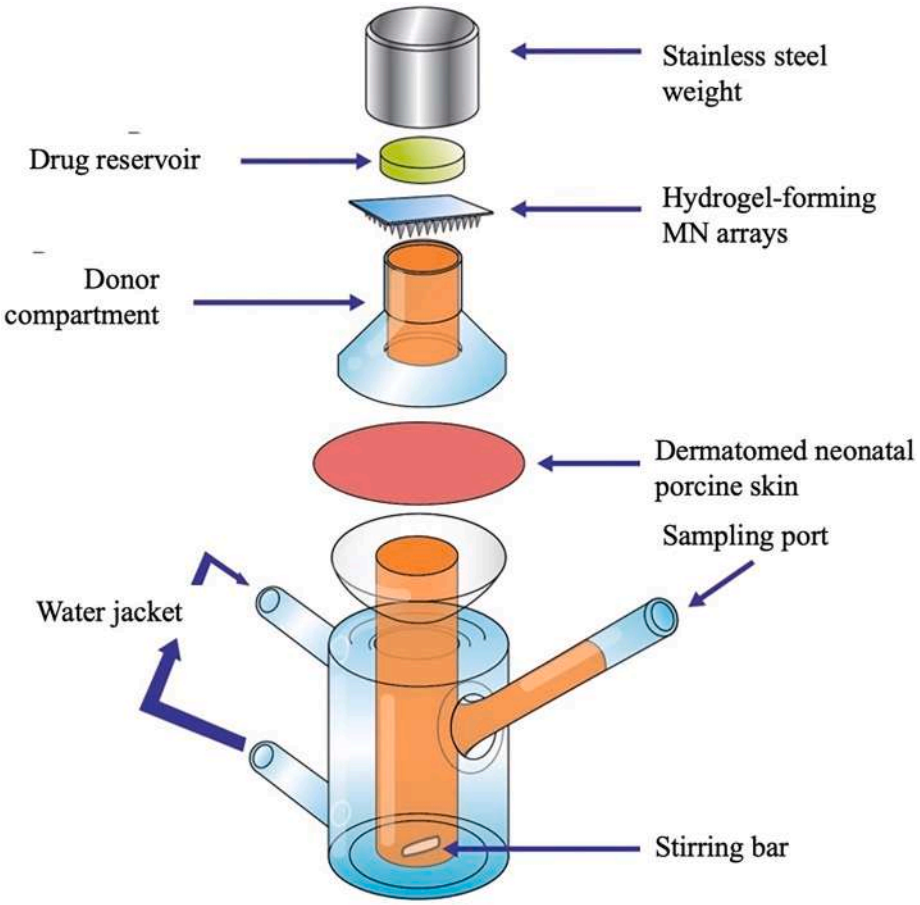

Fig. 3. Schematic illustration of modified Franz Cell chamber system for *in vitro* permeation studies of TB drugs loaded in reservoirs across neonatal porcine skin using hydrogel-forming MN arrays.

2.11. Reservoir characterisation

Morphology of LYO reservoirs was observed using the light microscope. A tablet tester (Dr. Schleuniger Pharmatron, Copley Scientific, Nottingham, UK) was used to determine the hardness of all reservoir formulations. Mechanical properties of PEG reservoirs were tested using the TA in compression mode. Dissolution times of all reservoir formulations were determined visually. Briefly, a reservoir was placed in 20 mL of appropriate release medium, agitated using a small magnetic bar (12 × 6 mm) at 600 rpm and maintained at 37 °C. Then, the time required for the reservoirs to fully dissolve was recorded as the dissolution time [23]. Moreover, differential scanning calorimetry (DSC) and fourier transform infrared (FTIR) studies of pure drug, pure excipients and reservoirs were performed using DSC Q100 (TA Instruments, Elstree, Hertfordshire, UK) and an attenuated total reflectance-fourier transform infrared (ATR-FTIR) spectrometer (Accutrac FT/IR-4100™, Perkin Elmer, USA), respectively.

2.12. In vitro permeation studies

The modified Franz diffusion cells (Permergear, Hellertown PA, USA) were used in order to assess the permeation of drug from the reservoir *via* hydrogel-forming MN arrays, across dermatomed neonatal porcine skin (Fig. 3) [18,41]. Skin samples were obtained from stillborn piglets and excised < 24 h after birth. Skin was excised as full thickness and then shaved carefully using a razor. Dermatomed skin was obtained by trimming shaved full thickness skin using an electric dermatome (Integra Padgett® model B, Integra Life Sciences Corporation, Ratingen, Germany) to a thickness of approximately 350 μm and then frozen at −20 °C until required. Prior to the experiment, the skin was pre-equilibrated in PBS pH 7.4 for 30 min. Two types of MN formulations were fabricated for permeation studies of drug reservoir. For all drugs, MN arrays were prepared from an aqueous blend of 20% w/w Gantrez® S-97, 7.5% w/w PEG 10,000 and 3% w/w Na_2CO_3. Another type of MN arrays was used for INH and PYR specifically, which was prepared from aqueous blends containing 15% w/w PVA, 10% w/w PVP and 1.5% w/w citric acid with a crosslinking time of 40 min at 130 °C. The MN arrays were inserted into the skin using firm finger pressure for 30 sec and then 20 μL of PBS pH 7.4 were placed on the top of the array to promote adhesion of the reservoir to the lower surface of the MN arrays. The selected reservoir formulation, based on the optimisation process, was placed on the top of the MN arrays already inserted into the skin. A 5.0 g stainless steel cylinder (diameter 11 mm) was placed on top of the reservoir and MN arrays to prevent their expulsion, after which the donor compartment was clamped onto the receiver compartment. For all drugs, excluding RIF, degassed PBS (pH 7.4) was added to the receiver compartment and pre-heated to 37 ± 1 °C to ensure complete contact between the fluid on the receiver compartment and the porcine skin. PBS (pH 7.4) containing 1% w/v SLS and 1% w/v AA was used as a release medium in the specific case of RIF in order to maintain sink conditions and prevent drug degradation. At pre-determined time intervals, 200 μL of dissolution media from the receiver compartment were removed using a syringe, replacing them with fresh pre-warmed medium. All samples were then analysed using a validated HPLC method, as described in Section 2.13.

2.13. Instrumentation and chromatographic condition for the analytical method

The individual quantification of RIF, INH, PYR and ETH was performed using HPLC. An Agilent technologies 1220 infinity compacted LC series consisting of Agilent degasser, binary pump, auto standard injector and detector (Agilent Technologies UK Ltd, Stockport, UK) was used for the analysis. Regarding ETH, due to the absence of strong chromophore groups, a pre-column derivatisation with phenyl ethyl isocyanate (PEIC) was applied to the samples prior to analysis. For derivatisation purpose, a 1.2 mL of ETH-containing sample was added into a tube containing 0.3 mL of PEIC (1.2 mg/mL) and mixed. It was shaken at 37 °C for 90 min before HPLC injection. Isocratic separations were achieved using a Phenomenex® Luna C_{18} (ODS1) column (150 mm × 4.6 mm internal diameter, 5 μm packing) (Phenomenex, Cheshire, UK). The injection volume was 50 μL and the analyses were performed at ambient temperature. The mobile phase, flow rate and UV detector used for each drug are presented in Table 3. The chromatograms were analysed using the Agilent ChemStation® Software B.02.01. The International Council of Harmonisation (ICH) 2005 guidelines were followed as a reference to assess all the analytical methods.

Table 3
Parameters of HPLC analysis for RIF, INH, PYR and ETH quantification.

Analyte	Mobile phase	Flow rate	UV detection
RIF	25 mM sodium dihydrogen phosphate buffer (with 1% v/v TEA, pH 6.8 adjusted using orthophosphoric acid) and methanol (30:70 v/v)	1 mL/min	334 nm
INH	Water and methanol (25:75 v/v)	1 mL/min	264 nm
PYR	Water and methanol (50:50 v/v)	1 mL/min	270 nm
ETH	25 mM sodium dihydrogen phosphate buffer (with 1% v/v TEA, pH 3.0 adjusted using orthophosphoric acid) and methanol (25:75 v/v)	1 mL/min	210 nm

2.14. Statistical analysis

Statistical analysis were performed using GraphPad Prism® version 8.0 (GraphPad Software, San Diego, California, USA). All experimental results were presented as means ± standard deviation (SD), unless otherwise stated. An unpaired *t*-test was used for comparison of two cohorts. One-way analysis of variance (ANOVA) was used for comparison of multiple cohorts. In all cases, $p < 0.05$ used to denote statistically significance, where *p*-value outputs were 0.033(*), 0.002(**) and <0.001(***).

3. Results and discussion

3.1. Swelling properties of hydrogel films

Swelling of hydrogels affects their mechanical characteristics and solute diffusion capability [30,42]. As presented in Fig. 4A, the result showed that films prepared from aqueous blends of Gantrez® S-97 (H1), known as super-swelling hydrogel-forming formulations, showed the highest swelling percentage when compared to PVA-based films ($p < 0.001$) [18]. Swelling properties of a hydrogel are based on the crosslinking ratio, polymer and crosslinker type [30,43]. Crosslinking ratio may be defined as the molar ratio of crosslinker to backbone polymer [43]. In this case, a higher crosslinking ratio in PVA-based films compared to Gantrez® S-97-based films leads to a lower swelling degree due to movement restriction of polymer chains by the highly crosslinked network [43]. Additionally, H1 contained a modification agent, Na_2CO_3, included to decrease the crosslinking degree and, hence, resulted in a looser network structure with a higher swelling degree when compared to PVA-based formulations. Moreover, the higher content of carboxyl acid groups (pKa = 4–5) in the uncross-linked Gantrez® S-97 copolymer within H1 yielded a to higher swelling degree of film formulations compared to H2 and H3, which both are PVA-based formulations. When the dried film was placed in PBS pH 7.4, free Gantrez® S-97 dissociated, promoting the carboxylic acid group to be ionised [44]. The presence of more ionisable groups within film formulations resulted in more cation attraction within the network, leading to raising electrostatic repulsion, which in turn increases chain relaxation, absorbing

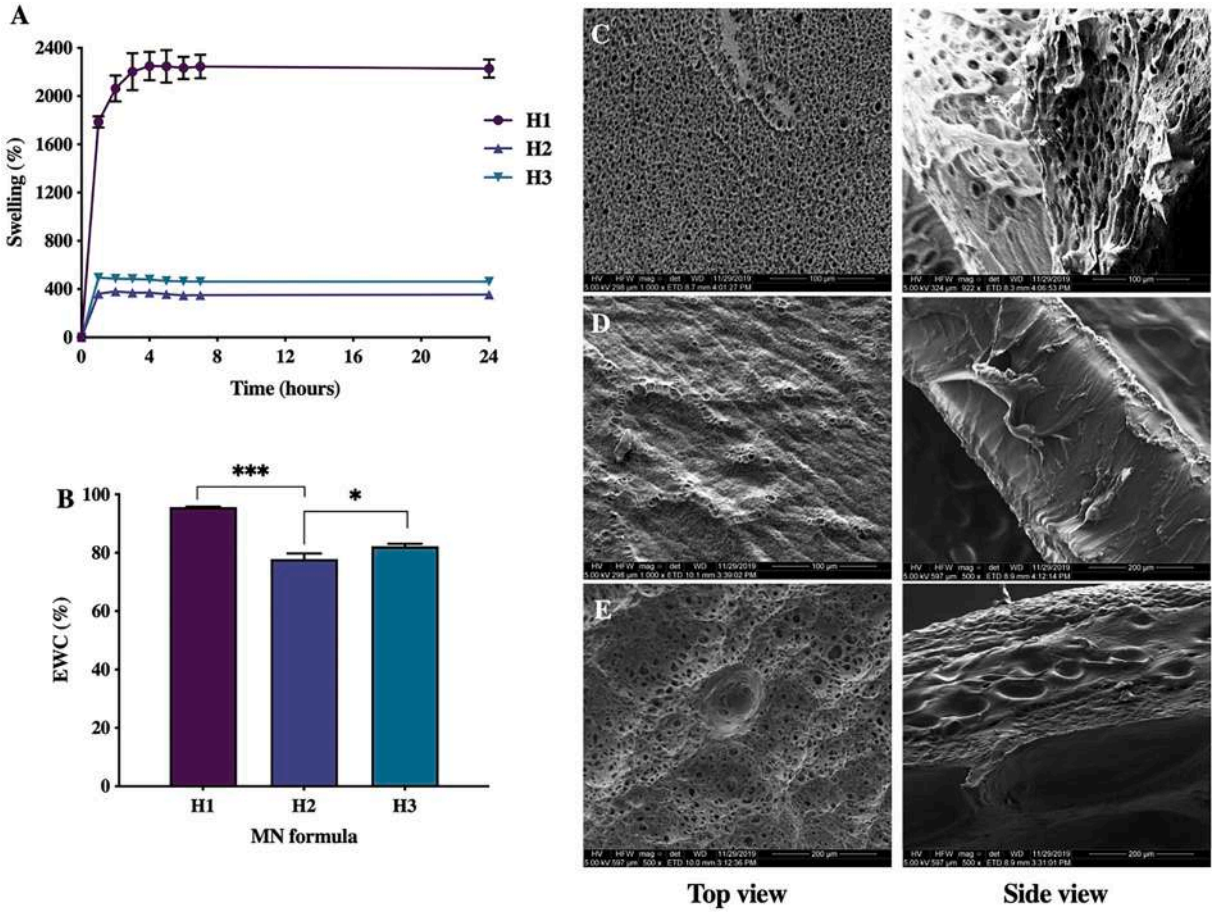

Fig. 4. (A) Swelling (means ± SD., n = 3) and (B) EWC percentage of hydrogel films over 24 h (means + SD., n = 3). SEM micrographs of representative swollen hydrogel film morphology after exposure to pH 7.4 buffer, including (C) formulation prepared from aqueous blend containing 20% w/w Gantrez® S-97, 7.5% w/w PEG 10,000 and 3% w/w Na_2CO_3; formulation prepared from aqueous blend containing 15% w/w PVA, 10% w/w PVP and 1.5% w/w citric acid with the crosslinking time of (D) 3 h and (E) 40 min, respectively.

more water to be included in the stretched network [43–46]. By comparing between the same formula (15% w/w PVA, 10% w/w PVP and 1.5% w/w citric acid) with different crosslinking time, the swelling percentage of H2 was significantly lower than H3 ($p < 0.001$). This is probably due to higher ester link formation between PVA and citric acid during the extended heating time. Similar trends were observed by previous studies, extending the crosslinking time contributes to higher crosslinking degree, thus lowering the swelling degree [44,47].

The water uptake capability was determined based upon the percentage equilibrium water content (EWC) of the films. As predicted, the film prepared from H1, containing Gantrez® S-97, exhibited the highest EWC percentage compared to PVA-based formulations ($p < 0.001$) (Fig. 4B). Furthermore, a significant difference of EWC percentage was found between H2 and H3 ($p < 0.033$). Both formulations were cast from aqueous blend containing 15% w/w PVA, 10% w/w PVP and 1.5% w/w citric acid. Considering the swelling percentage results, a similar pattern was found for the EWC percentage. Extending heat-treatment duration between PVA and citric acid led to the formation of a more highly crosslinked system, resulting in a lower swelling percentage, as less water can be incorporated into the hydrogel network [48].

3.2. Morphology of hydrogel-forming films

SEM images of the hydrogel films are presented in Fig. 4C-E where the porous properties of the hydrogels can be seen. H1 prepared from the aqueous blends containing Gantrez® S-97 exhibited more porous structures compared to the PVA-based films (H2 and H3). These results were in agreement with both swelling and EWC percentages. With respect to the same formulation, and besides the crosslinking time, the higher swelling degree of H3 compared to H2 was well explained by the obtained SEM images (Fig. 4D-E). This might confirm that the higher crosslinking degree found in H2, due to the extended crosslinking time, resulted in a less porous structure within the film formulation compared to H3.

3.3. Solute diffusion studies

Fig. 5A-D presents the permeation of RIF, INH, PYR and ETH across the equilibrium swollen hydrogel-forming films using side-by-side diffusion cells. The film formulation prepared from Gantrez®-S97 was found to be beneficial to the permeation of hydrophobic substances, in this case RIF, due to its characteristics of higher water-containing capacity and higher porosity within the hydrogel compared to PVA-based formulations. As a consequence, the mobility of RIF molecules becomes unrestricted within the hydrogel network [48]. A similar result was attained from ETH, the permeation was significantly higher through the Gantrez®-S97-based film, which might be attributed to its high solubility in water ($p < 0.001$). ETH solute transport within a hydrogel will occur primarily within the fluid-filled space between the polymer chains. H1 is able to retain a higher amount of water compared to both H2 and H3. Therefore, more ETH molecules can be dissolved, permeating across the swollen hydrogel film [49]. In both INH and PYR cases, the solute permeability was mostly controlled by diffusing species, possible leading to solute-gel interaction between amine groups of

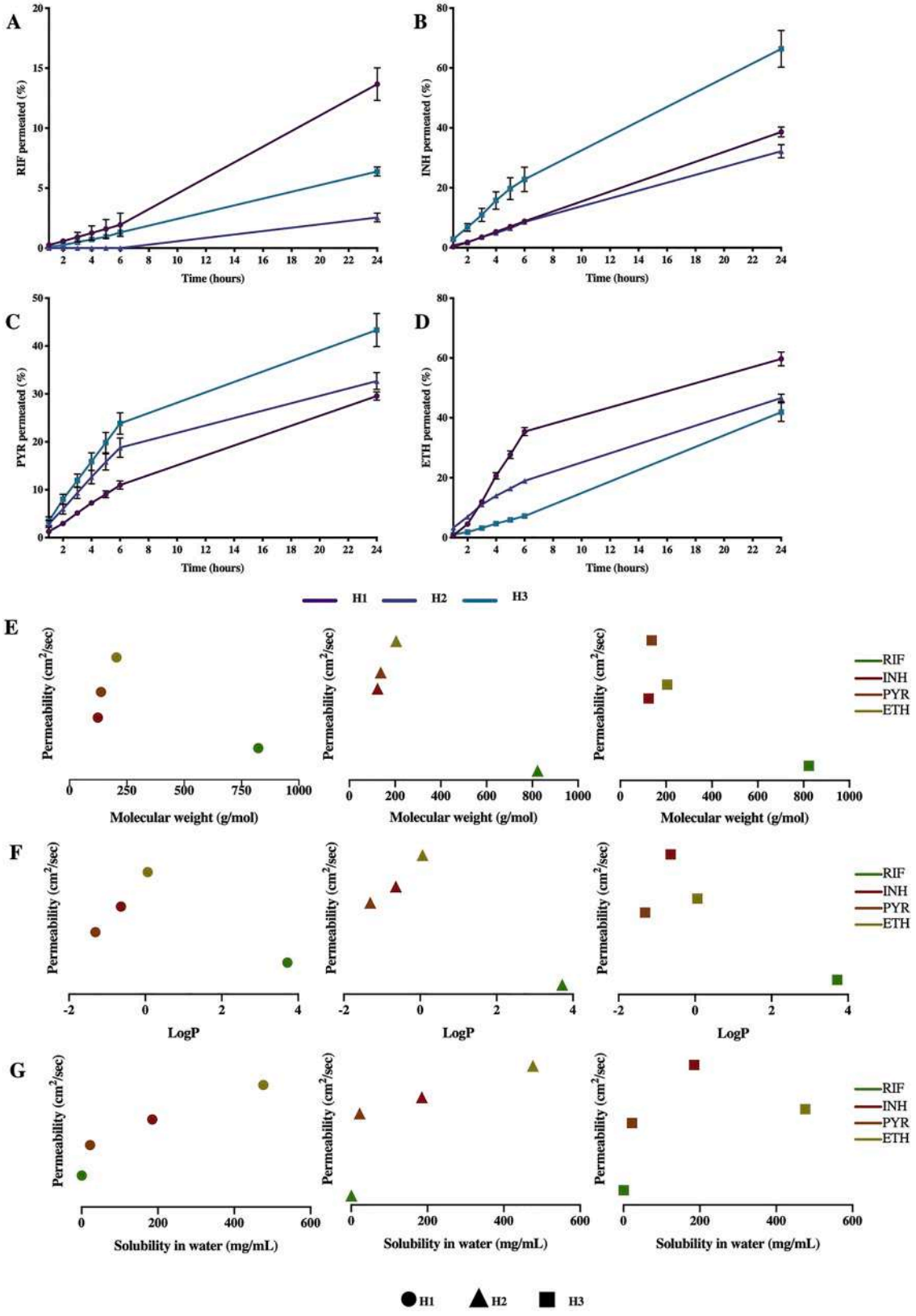

Fig. 5. Permeation percentage of (A) rifampicin, (B) isoniazid, (C) pyrazinamide and (D) ethambutol across pre-swollen hydrogel membranes (means ± SD., n = 3). Solute permeability through swollen hydrogel film associated with (E) molecular weight, (F) logP and (G) aqueous solubility. H1 prepared from aqueous blend containing 20% w/w Gantrez® S-97, 7.5% w/w PEG 10,000 and 3% w/w Na_2CO_3; H2 and H3 were prepared from aqueous blend containing 15% w/w PVA, 10% w/w PVP and 1.5% w/w citric acid with the crosslinking time of 3 h and 40 min, respectively.

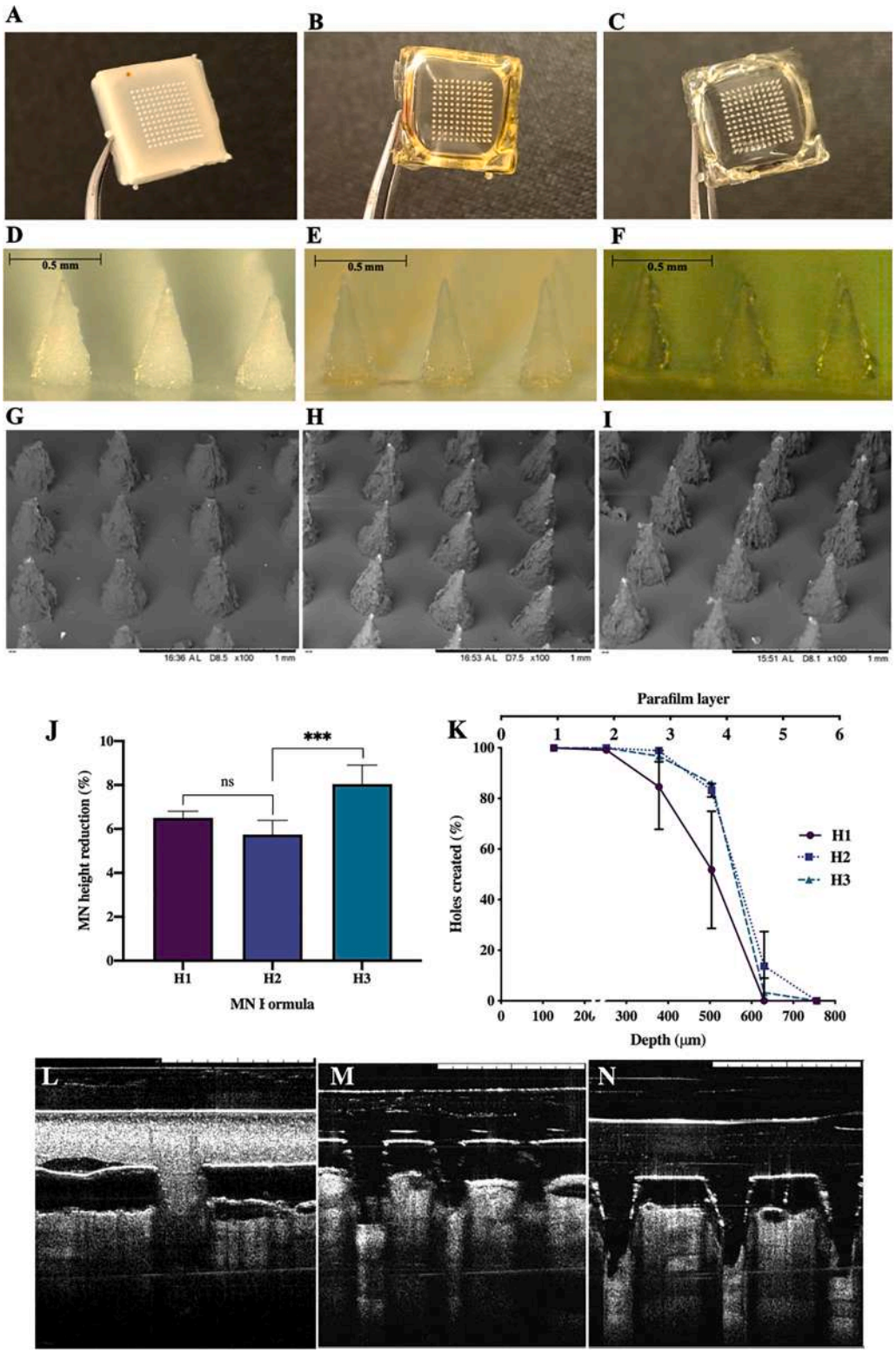

Fig. 6. Images of hydrogel-forming MN arrays composed of 121 needles, in conical shape, 600 μm height, 300 μm width at the base, and 300 μm interspacing. (A) Digital images of hydrogel forming formulation prepared from aqueous blend containing 20% w/w Gantrez® S-97, 7.5% w/w PEG 10,000 and 3% w/w Na_2CO_3 (H1). Formulation prepared from aqueous blend containing 15% w/w PVA, 10% w/w PVP and 1.5% w/w citric acid with the crosslinking time of (B) 3 h (H2) and (C) 40 min (H3), respectively. Microscopic images of hydrogel-forming formulation prepared from (D) H1, (E) H2 and (F) H3. SEM images of hydrogel forming formulation prepared from (G) H1, (H) H2 and (I) H3. (J) Comparison of height reduction percentage of MN arrays needles followed application of force 32 N using TA (means + SD., n = 6). (K) Percentage of holes created in each Parafilm®M layer and estimate insertion depths following insertion of hydrogel-forming MN array formulations (means ± SD., n = 3). Representative OCT images of hydrogel-forming MN arrays prepared from (L) H1, (M) H2 and (N) H3. The white scale bar represents a length of 1 mm.

solute and carboxylic acid group of free Gantrez®-S97 co-polymer within the hydrogel network. In turn, solute entrapment in the gel system of H1 inevitably occurred [48,50]. Higher permeation percentage of both INH and PYR across the PVA-based film than Gantrez®-S97-based film suggest that amine groups of solute were preferably excluded from the uncharged gel network (PVA-based formulation) [48,51].

The relation between permeability coefficient of the hydrogel formulations and several solute properties, namely molecular weight, polarity (logP) and solubility are shown in Fig. 5E-G. The increasing molecular weight and logP of solute was followed by increasing permeability coefficient for all hydrogel formulations. However, this simplified pattern will be only for small size solute with hydrophilic properties. In contrast, the relationship between permeability and nonpolar solute can be more complex due to the hydrophobic interactions, as the most common contributing factor, that possibly occurred [48]. For instance, nonpolar solutes could interact with the polymer backbone of the hydrogel, causing the solute entrapment within the hydrogel network [48,52,53]. Moreover, it is apparent that hydrogel permeability increases as solute solubility is increased. Because water-contained of hydrogel network, it is expected that a more hydrophilic solute is more likely to be increasingly excluded from the hydrogel system [48]. Accordingly, the hydrogel permeability can be tailored for a specific drug delivery application by varying the polymer used as hydrogel backbone and crosslinking degree of the formulation to achieve a maximum solute diffusion. In terms of TB drug delivery, due to the different nature of TB drugs as previously discussed, a distinctive hydrogel formulation was required to increase the drug release from reservoir through hydrogel-forming MN array. Reservoirs of RIF and ETH were incorporated on top of hydrogel-forming MN arrays prepared using aqueous blends of 20% w/w Gantrez® S-97, 7.5% w/w PEG 10,000 and 3% w/w Na_2CO_3 (H1). Furthermore, formulation prepared from 15% w/w PVA, 10% w/w PVP and 1.5% w/w citric acid with 40 min of crosslinking time (H3) were combined with INH and PYR reservoirs for further *in vitro* permeation studies.

3.4. Fabrication and characterisation of hydrogel-forming MN arrays

The digital and SEM images of hydrogel-forming MN arrays are presented in Fig. 6A-I. All MN arrays prepared exhibited homogeneous polymer distribution with the resultant MN arrays having sharp needle tips.

Compression resistance testing was performed to ensure that the MN arrays were capable of penetrating the *stratum corneum*. Height reduction percentage of the MN formulations was calculated following the application of 32 N for each array equal to insertion force reported to be applied with a thumb by patients [38]. As displayed in Fig. 6J, H3 MN arrays exhibited the highest percentage of needle height reductions ($p < 0.001$). This result could be explained by a shorter crosslinking time which, in turn, led to a softer material. These results provide an important insight into the MN arrays capability to resist a compression force, showing the formulations had reasonable mechanical strength, with approximately <10% reduction in needle height observed [54].

As presented in Fig. 6K, all formulations inserted into the first four layers of Parafilm®M. As the mean thickness of one layer of Parafilm® M is about 125 μm, it can be assumed that all MN arrays were inserted to a minimum depth of 504 μm, accounting for approximately 84% of MN height. Thus, the needle height inserted in the Parafilm® M was similar to the values previously reported [19,54–56]. Additionally, as presented in Fig. 6L-N, the MN arrays exhibited penetration depths of 451.45 μm, 429.15 μm and 408.10 μm in full-thickness neonatal porcine skin for H1, H2 and H3 respectively. The needle height that inserted into the skin model was similar to values previously obtained [54,55]. The insertion depth was found to be not statistically different by comparing the PVA based-formulations with the Gantrez® S-97-based formulation ($p > 0.05$). Hence, results from the insertion study demonstrate the potential of hydrogel-forming MN arrays prepared from PVA-based formulations for transdermal drug delivery.

Table 4
Critical process temperature of several excipients used in LYO reservoir formulation.

Excipient	Tg′ (°C)	Tc (°C)	References
Sucrose	−32, −35	−34, −32	[63–65]
Mannitol	−35, −28	NA	[63,66]
Glycine	−62	NA	[67]
Trehalose	−27, −29	−29.5, −34	[63,65,66]
Gelatin	−9	−8	[68]

3.5. Preparation and optimisation of lyophilised reservoirs

Preliminary study results, as presented in Fig. S1 (supplementary information), exhibited that different bulking agent was required for each drug-containing lyophilised reservoir formulation. RIF LYO reservoirs prepared using trehalose as bulking agent, required the shortest time to dissolve when compared with the rest of formulations ($p < 0.05$). Moreover, the dissolution time of both INH and PYR LYO formulations were found to be significantly different for reservoirs prepared using sucrose compared to other bulking agents at a low concentration (2% w/w) ($p < 0.05$). This may be related to the higher solubility of both sucrose and trehalose, which have amorphous properties, compared to both mannitol and glycine, which have crystalline structures [57,58]. During LYO reservoir preparation, crystalline bulking agents can form a strong crystal structure between molecules. Hence, they require a higher energy to disintegrate and dissolve [59,60].

In the case of ETH, all LYO formulations collapsed after finishing the lyophilisation process. This could possibly be triggered by the melting point of ETH (88 °C), which is lower than the boiling point of water. Therefore, causing ETH incapability to withstand the drying condition and resulting in the loss of cake integrity structure during the water removal process [61]. Moreover, the addition of a bulking agent into the ETH reservoir formulation failed in forming a robust LYO cake. This might be related to the critical temperature of the aqueous mixture composed of ETH and bulking agent, since it was lower when compared to the aqueous mixture prepared without a bulking agent. The critical temperature is defined as the maximum temperature where a LYO cake can maintain its integrity [62]. The critical temperature for crystalline systems is closely related to the glass transition temperature (Tg'), whilst for amorphous systems is represented by both Tg' and collapse temperature (Tc) [62]. The critical temperature of several excipients used in LYO reservoir formulations is presented in Table 4. It can be seen that the Tg' and Tc values of all the bulking agent used are much lower than gelatin. Hence, the presence of bulking agents in the ETH LYO formulation decreased the critical temperature of ETH.

In order to improve the collapse issue, several iterations were investigated regarding gelatin concentration and the total mass of LYO reservoirs. In addition to this, the total mass of LYO formulation was varied by changing the amount of water in the formulation, which could also affect the duration of the drying process. The dissolution time of ETH containing LYO reservoirs is displayed in Fig. S2 (supplementary information). A LYO reservoir formulation of 100 mg containing 2.5% w/w of gelatin led to a homogeneous and robust reservoir. Moreover, it showed the shortest time to dissolve in the release medium in comparison to all other formulations.

Based on preliminary results, trehalose for RIF and sucrose for INH and PYR were selected as a bulking agent to be used in the optimisation process using the CCD system. The concentration of drug, gelatin and bulking agent were used as the formulation factors that needed to be optimised. There were 14 formulations for the optimisation process suggested by the software, which are presented in Table S5, Table S6 and Table S7 (supplementary information) for RIF, INH and PYR, respectively. The representative 3D graphs describing the effect of selected

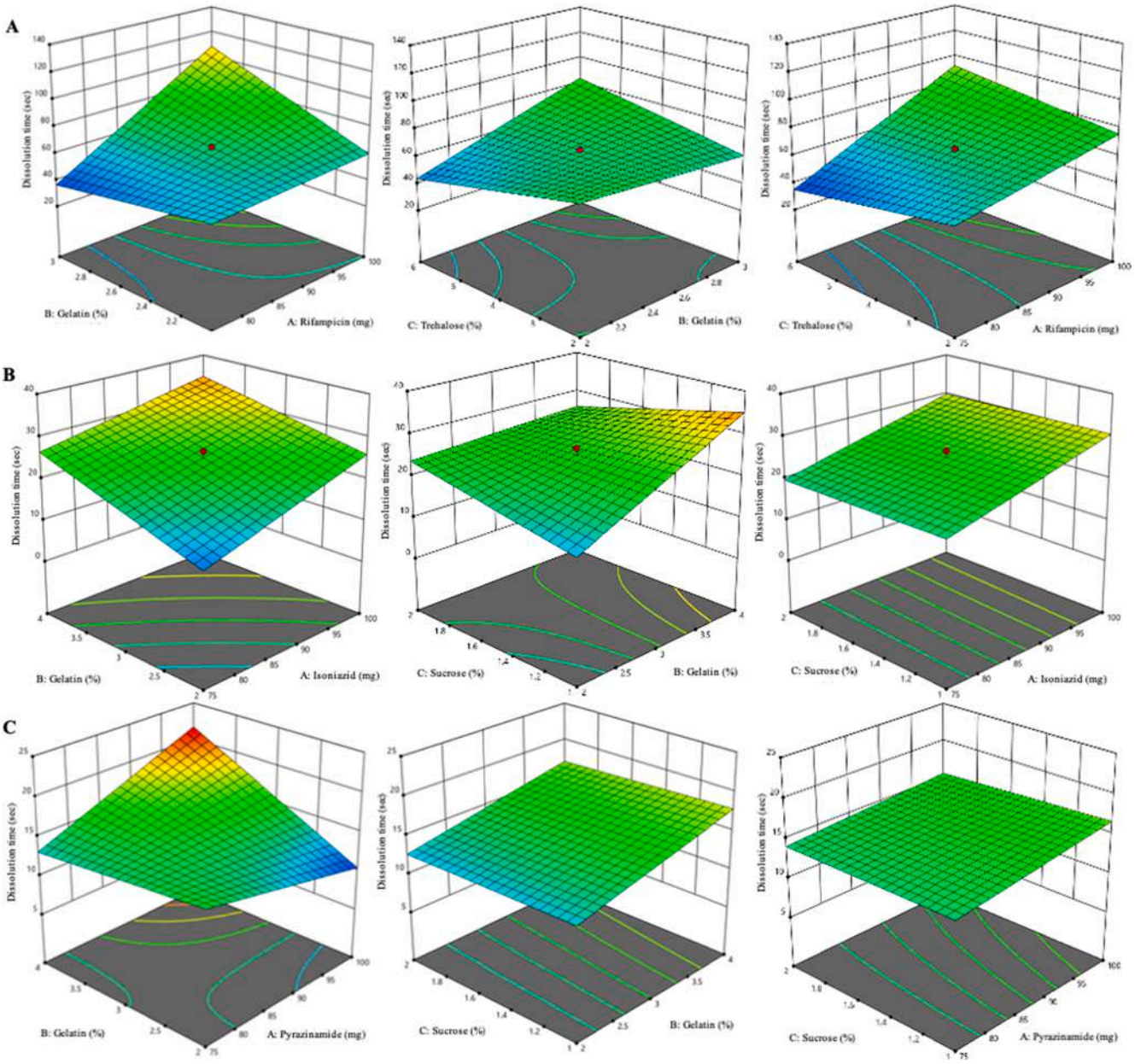

Fig. 7. Response surface plots describing the effect of drug, gelatin and bulking agent concentration on the dissolution time parameter of each (A) RIF, (B) INH and (C) PYR LYO reservoir formulations.

parameters on the dissolution time and hardness are presented in Fig. 7 and Fig. 8, respectively. Optimised formulations based on the output of software analysis were selected and prepared for final characterisation studies. Several optimised formulations were generated by the software and, then, ranked based on the desirability factor. The optimum formulations for RIF, INH and PYR were chosen by considering the highest desirability factor, obtained from the analysis output. The selected formulation for each drug was prepared to investigate dissolution time and hardness of the obtained reservoirs. Table 5 presents the predicted and observed values of dissolution time and hardness for the optimised formulations. The bias value of optimised formulations in all cases was $< 15\%$, indicating that the optimisation process of LYO reservoir formulation was successful [54].

3.6. Characterisation of lyophilised reservoirs

The final RIF, INH, PYR and ETH LYO formulations were all homogeneous and robust, as presented in Fig. 9A-D. FTIR analysis (Fig. 9E) showed that the highlighted functional groups of pure RIF, INH, PYR and ETH, detailed in Table 6, were similar to those obtained in the FTIR spectra of drug-containing LYO formulations. Thus, there was no detectable excipient interaction with RIF, INH, PYR or ETH in the LYO formulations. The thermogram profiles of RIF, INH, PYR, ETH, and their respective LYO formulations, are presented in Fig. 9F. The DSC thermogram of both pure RIF and RIF containing LYO reservoirs showed an endothermic peak at 191 °C, followed by an exothermic peak at 259 °C. These two peaks are attributed to RIF polymorphism, as previously discussed by Alves et al. [69]. A sharp endothermic peak for both INH and PYR was found at 176 °C and 194 °C, respectively. For the pure ETH thermo profile, two endothermic peaks appeared at 75 °C and 202 °C [70]. It is important to note that the endothermic peak at 75 °C is related to the low critical temperature of ETH. As the critical temperature of ETH is lower than water's triple point, the cake collapsing during the lyophilization process was inevitable. Moreover, a small peak

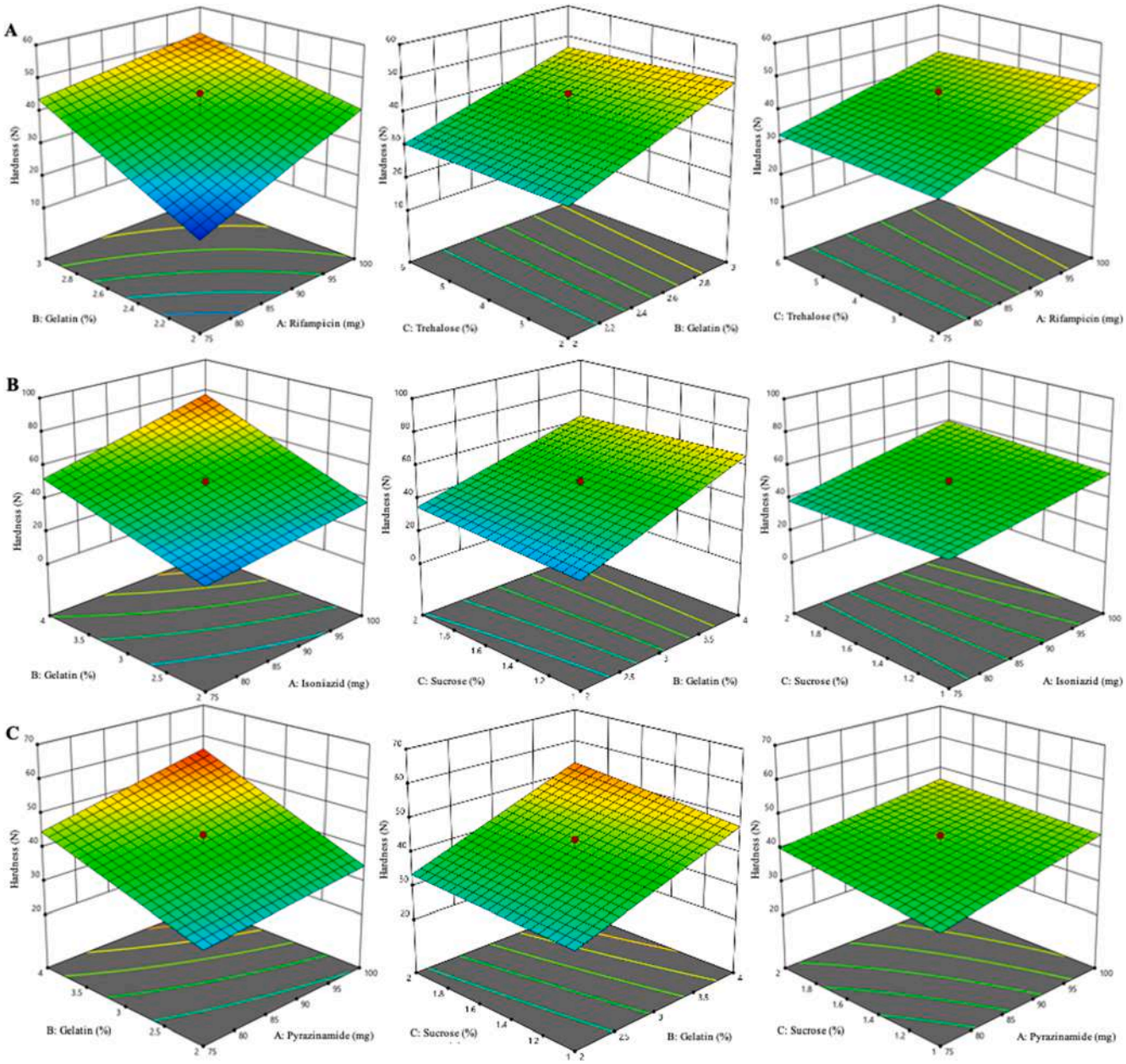

Fig. 8. Response surface plots describing the effect of drug, gelatin and bulking agent concentration on hardness parameter of (A) RIF, (B) INH and (C) PYR LYO reservoir formulations.

Table 5
Predicted and observed responses of LYO reservoirs formulation.

Drug	Factors			Responses	Predicted	Observed (mean ± SD, n = 3)	Bias (%)
	Drug concentration (mg)	Gelatin concentration in aqueous mixture (%w/w)	Bulking agent concentration in aqueous mixture (%w/w)				
RIF	75	2.39	2.00	Dissolution time (sec)	34.32	32.67 ± 1.41	−4.83
				Hardness (N)	30.00	29.65 ± 5.65	−3.33
INH	75	2.29	1.00	Dissolution time (sec)	12.63	12.00 ± 0.70	−5.03
				Hardness (N)	30.00	31.67 ± 1.41	−5.55
PYR	100	2.00	2.00	Dissolution time (sec)	10.10	11.33 ± 2.12	12.20
				Hardness (N)	38.29	39.33 ± 0.70	2.72

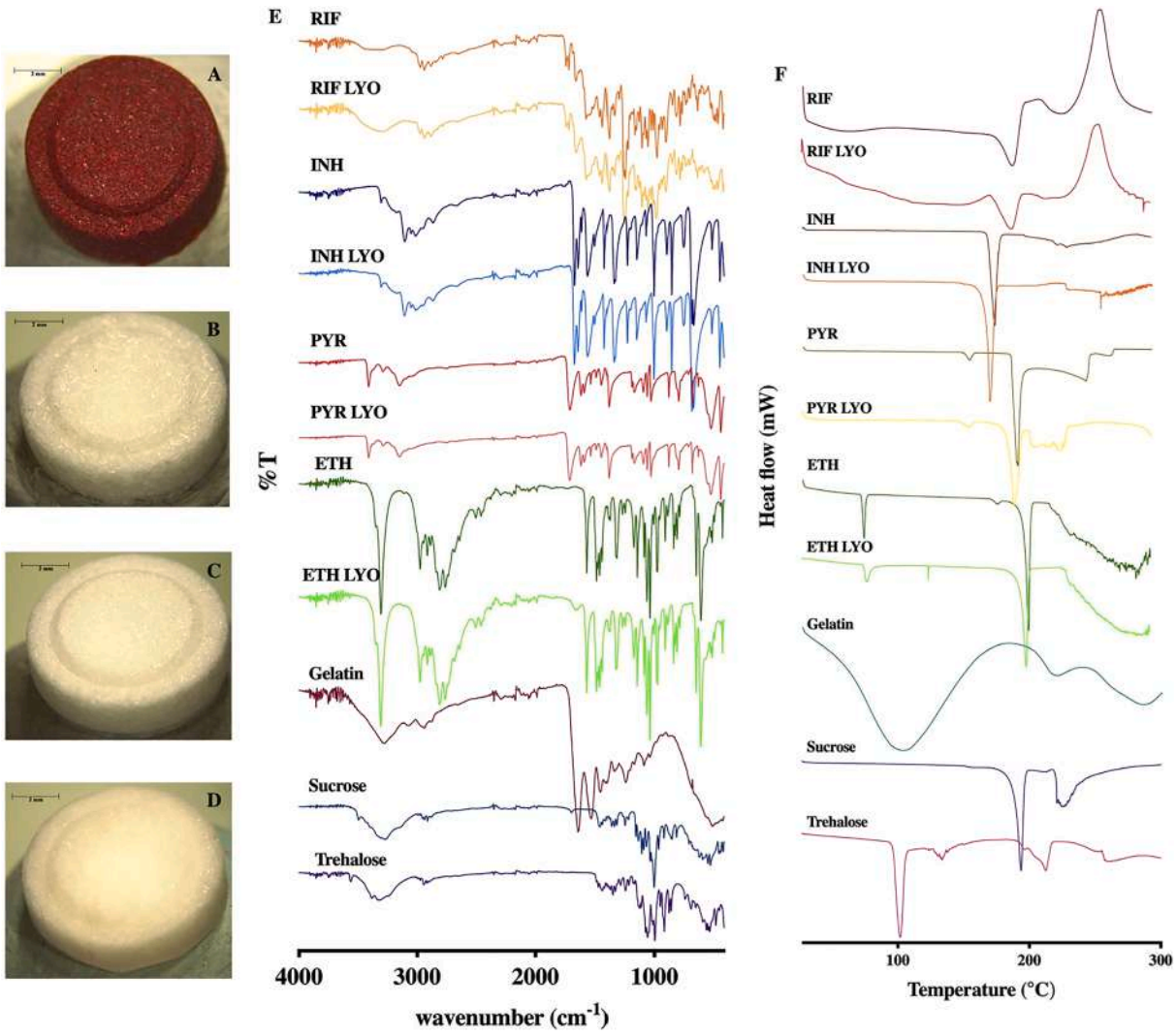

Fig. 9. Physical appearance of (A) RIF, (B) INH, (C) PYR and (D) ETH LYO reservoir formulations. Representative (E) IR spectra and (F) DSC thermogram of pure drug, optimised formulation of LYO reservoir formulations and pure excipients, including gelatin, sucrose and trehalose.

Table 6
Characteristic IR absorption of functional groups RIF, INH, PYR and ETH.

RIF	INH	PYR	ETH	Assignment
Wavelength (cm^{-1})				
3524–3629	3303	3402	3300	Primary O—H group
	3291	3267		Primary N—H group
	3091	2930	2969	C—H stretching
2768				H—C═O: C—H stretch
1706				C═O stretch
	1543	1579	1557	N—H bend
	1329	1379		NH_2 waging
1235	1219			N—N stretch
			1053	C—O stretch

appeared at 124 °C in the ETH LYO formulation, suggesting a new collapse temperature due to the presence of gelatin that increased the critical point to the higher temperature. It is notable that there a minor shifting of the peak was found in the thermogram of LYO reservoir formulation of each RIF, INH and PYR compared to each pure drug. During the lyophilisation process, there is a possibility for sucrose and trehalose to form hydrogen bond with drug through a direct interaction in order to replace the removed water [71].

3.7. Preparation and optimisation of direct compressed tablet

In this study, both disintegrant (sorbitol and mannitol) and super-disintegrant (crospovidone and SSG) were screened for DCT preparation. The results of preliminary disintegrant screening are presented in Fig. S2 (supplementary information). The dissolution time of DCT reservoirs prepared using crospovidone and SSG as super-disintegrant are significantly faster than the DCT reservoirs prepared using sorbitol and mannitol ($p < 0.05$). Moreover, the results showed that the DCT formulation prepared using crospovidone required the shortest dissolution time compared to the formulations prepared with other disintegrating and, hence, crospovidone was selected as the disintegrant for further optimisation process ($p < 0.05$). With respect to ETH, no significant difference in dissolution times were found in all the DCT formulations ($p > 0.05$). This may be related to the high solubility properties of ETH. Therefore, DCT reservoirs of ETH were prepared by compressing the pure powder of ETH, without any excipients.

The formulation optimisation was carried out using CCD and nine formulations were suggested to optimise the DCT reservoir. Response factors for RIF, INH and PYR are presented in Tables S8, S9 and S10 (supplementary information), respectively. The representative 3D surface graphs describe the parameter effect on the responses as displayed in Fig. 10A-B. The optimised formulations based on the output of software analysis were selected and prepared for their final

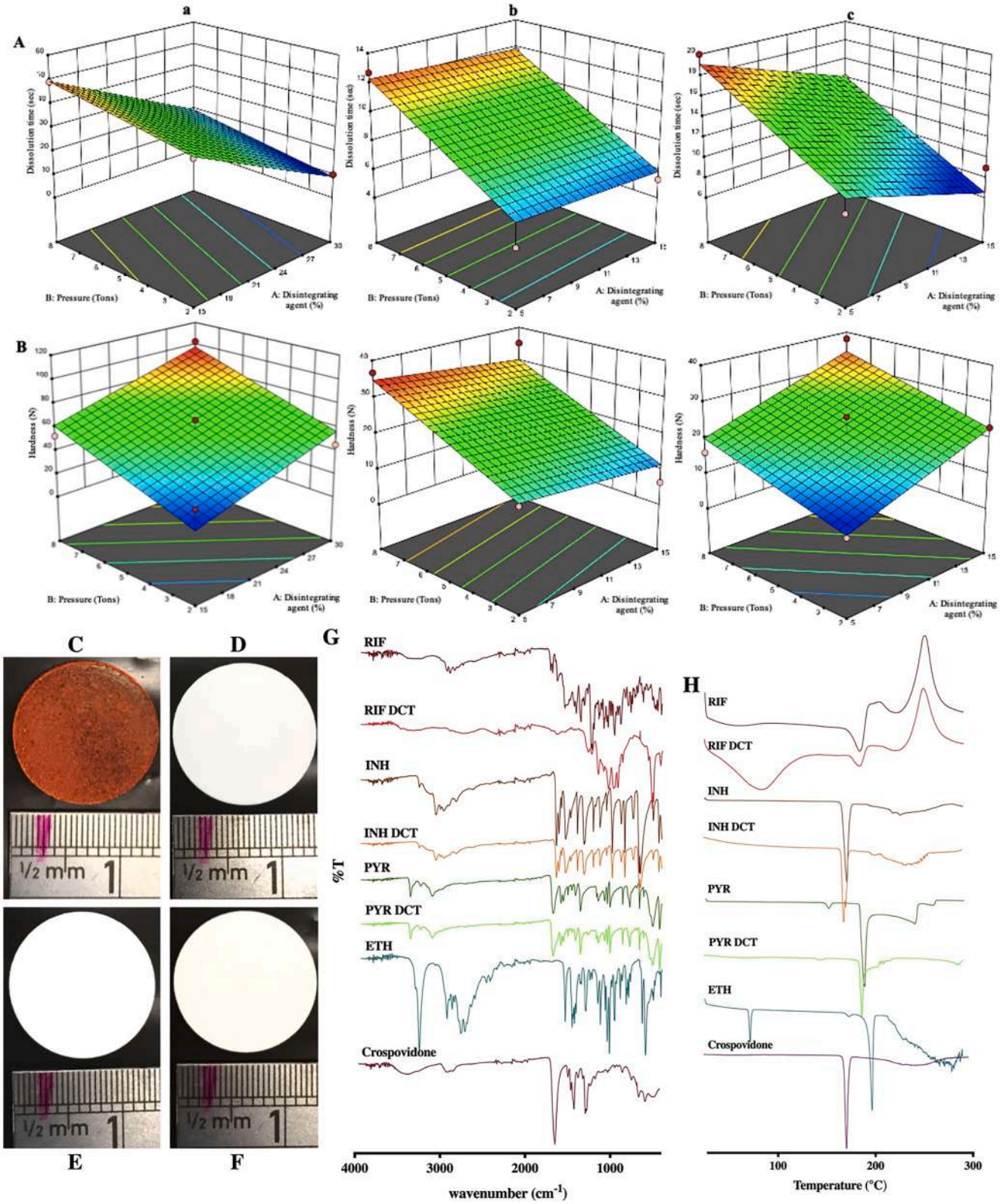

Fig. 10. Response surface plots describing the effect of disintegrating agent concentration and compression pressure to the (A) dissolution time and (B) hardness of (a) RIF, (b) INH and (c) PYR loaded in DCT formulations. Physical appearance of the optimised DCT formulation of (C) RIF, (D) INH, (E) PYR, and (F) DCT of ETH which was prepared exclusively by pure powder of ETH. Representative of (G) IR spectra and (H) DSC thermogram of pure drug, optimised formulation of DCT reservoir formulations and pure excipients, including crospovidone.

Table 7
Predicted and observed responses of the DCT optimum formulation of RIF, INH and PYR.

Drug	Factors		Responses	Predicted	Observed (mean ± SD, n = 3)	Bias (%)
	Disintegrant (%w/w)	Pressure (tonnes)				
RIF	30	7.49	Dissolution time (s)	9.46	10.67 ± 1.41	12.71
			Hardness (N)	56.87	58.00 ± 10.60	1.97
INH	5	6.50	Dissolution time (s)	10.79	12.00 ± 4.94	11.16
			Hardness (N)	30.00	33.00 ± 2.82	10.00
PYR	15	5.76	Dissolution time (s)	11.28	11.33 ± 4.24	0.41
			Hardness (N)	30.00	33.33 ± 6.36	11.11

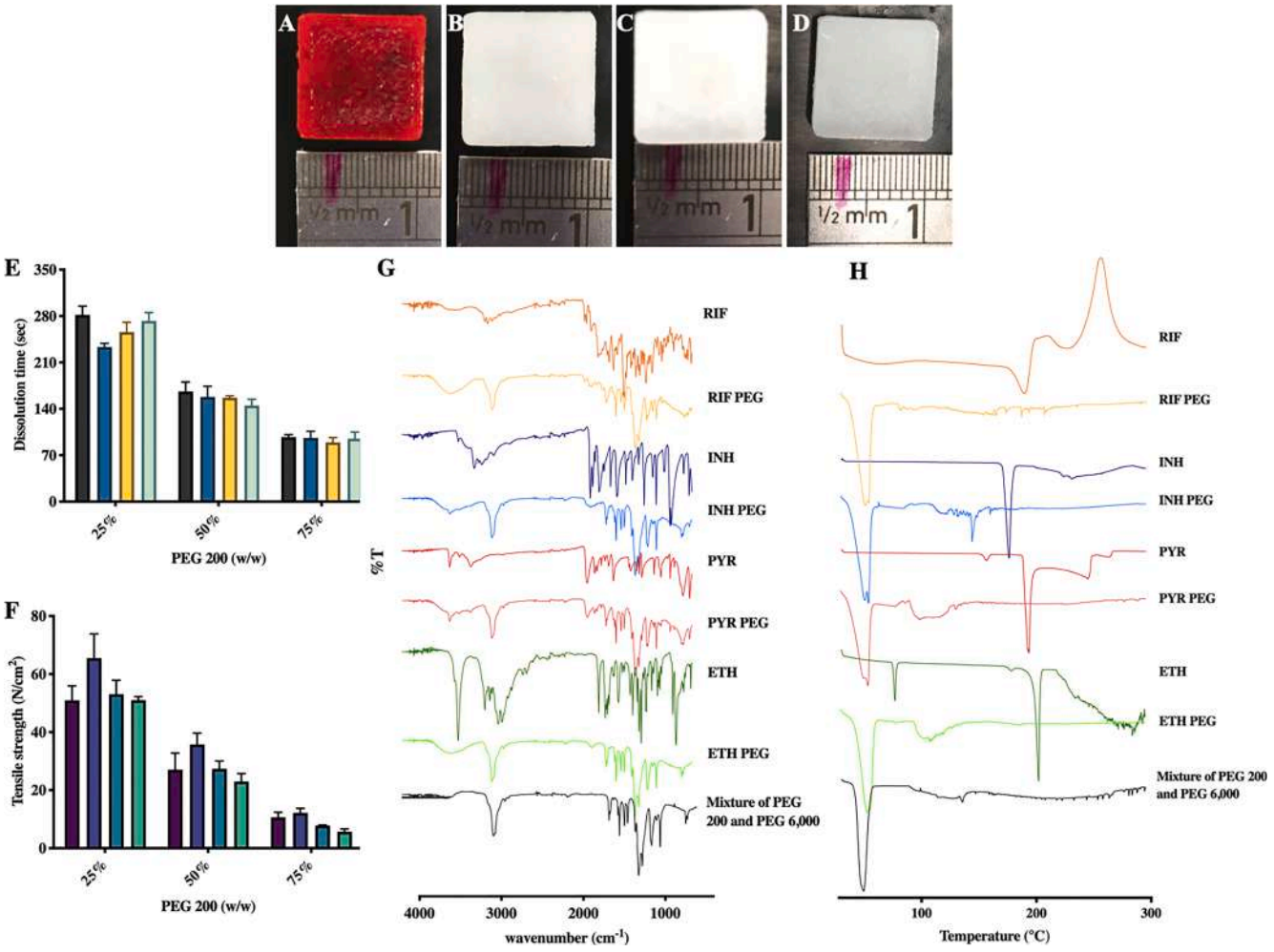

Fig. 11. Solid dispersion of (A) RIF, (B) INH, (C) PYR and (D) ETH PEG reservoir formulations. Comparison of (E) the dissolution time and (F) mechanical strength of PEG reservoir prepared (means + SD, n = 3). The representatives (G) IR spectra and (H) DSC thermogram of pure drug, selected PEG reservoir formulations, and mixture of PEG 6,000 and PEG 200.

characterisation. Two criteria were set in order to achieve optimum formulations, which were a minimum dissolution time and a DCT hardness greater or equal to 30 N [72,73]. One optimum formulation for RIF, INH and PYR was selected based on the highest desirability factor generated by the software. As shown in Fig. 10C-F, optimised formulations for each drug produced homogeneous and robust DCT. The dissolution time and hardness values are presented in Table 7, where it can be seen as percentage of bias <15%, demonstrating the success of the software optimisation process.

3.8. Characterisation of direct compressed tablets

The final DCT formulations containing RIF, INH, PYR and ETH were all homogeneous and robust in appearance, as shown in Fig. 10C-F. Furthermore, Fig. 10G illustrates the FTIR spectra of RIF, INH, PYR and ETH DCT formulations. There were no changes in the distinctive functional groups of RIF, INH, PYR and ETH when incorporated into their representative DCT formulations. Hence, there were no compatibility issues with the different excipients. The thermogram profiles of RIF, INH, PYR, ETH and their respective DCT formulations are presented in Fig. 10H. The results showed that there was a minor shifting in the peak of DCT formulation compared to each pure drug of RIF, INH and PYR. This may be possibly due to the compaction during the compression process, increase the density of both drug and crospovidone throughout the powder mixture, resulting intermolecular interactions and crystal state modification [74].

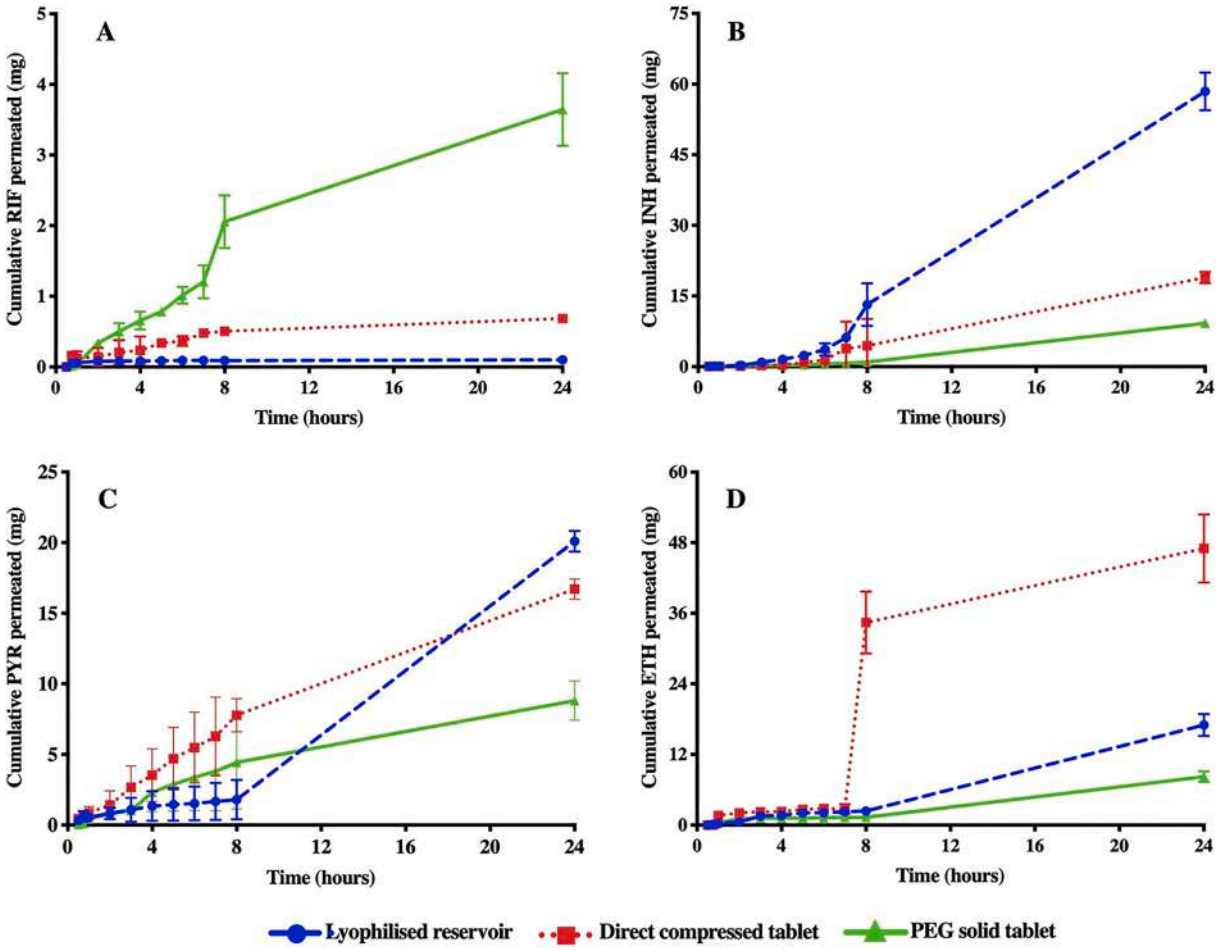

Fig. 12. In vitro permeation profiles of RIF (A), INH (B), PYR (C) and ETH (D) from drug reservoirs which incorporated on hydrogel-forming MN arrays (means ± SD, n = 3). Gantrez® S-97 based formulation (H1) was combined with RIF and ETH reservoirs whilst PVA-based formulation (H3) was integrated with INH and PYR reservoirs.

3.9. Preparation and evaluation of poly(ethylene glycol) solid reservoirs

Solubility of each drug in the PEG cosolvent candidates was studied, and the results are shown in Fig. S3 (supplementary information). The result revealed that PEG 200 was found to be most effective, increasing the solubility of all the drugs. Therefore, PEG 200 was chosen as a cosolvent for further PEG reservoir preparation. Different combinations of PEG 200 and PEG 6,000 were used to produce solid and uniform reservoirs (Fig. 11A-D). All formulations of drug-containing PEG reservoir were also characterised in terms of dissolution time and mechanical strength (Fig. 11E and Fig. 11F, respectively). With regards to the dissolution time, it was observed that an increase in PEG 200 proportion was followed by a significant reduction in the dissolution rate ($p < 0.05$). This result indicated that the reservoir SD system was strongly dependent on the proportion of PEG 200 and PEG 6,000. Drug dissolution is correlated with the rate of solute drug diffusion from the reservoir to the aqueous medium and, hence, affecting the rate of drug molecule solubilisation due to the interfacial tension [75].

Compression testing was used to determine the mechanical properties of the prepared reservoirs. The reservoir robustness is a key factor to consider for the physical resistance during the manufacturing process and transport. As displayed in Fig. 11F, an increase in the PEG 200 proportion led to a decrease of the reservoir mechanical strength. Reservoirs composed of 25% PEG 200 were significantly stronger than all reservoirs containing a higher liquid PEG concentration for all the drugs used in this study ($p < 0.05$). As previously reported, the degree of PEG compaction is clearly associated with the molecular weight of the glycol [76]. In the current work, PEG 6,000 concentration governed the reservoir resistance to compression due to its high molecular weight, which possibly accounts for the total energy required to break the reservoir. During the compression, PEG reservoirs are likely to experience complex stresses, generating simultaneously particle rearrangement, elastic and plastic deformation, and hence, resulting in breaking the inter particulate bonds followed by a fracture [76]. Overall, the result of compression testing confirmed that all reservoir formulations had a sufficient mechanical strength. Moreover, reservoirs composed of 75% PEG 6,000 showed the highest strength. However, as the drug is dissolved in the liquid PEG, the total drug that can be loaded would be limited in such formulations. Therefore, regarding the drug loading and dissolution time, a reservoir formulation with 25% w/w PEG 6,000 was selected for further experiments.

3.10. Characterisation of poly(ethylene glycol) solid reservoirs

FTIR analysis showed a substantial difference between drug-containing PEG spectra and their pure drugs (Fig. 11G). Compared to the pure drug, the characteristic spectra of the selected SD formulations were found to be broader, less frequent and weaker. This possibly due to the inter particulate bonds formed between the drug and PEG in all formulations. Moreover, the thermograms of RIF, INH, PYR, ETH, and their respective PEG formulations are presented in Fig. 11H. All the peaks of the pure drug disappeared, as the thermogram was found typically similar to thermogram of PEG mixture. Also, DSC analysis suggested that the drug was dissolved in the PEG matrix upon the SD

Table 8
Drug permeated from hydrogel-forming MN arrays combined with drug reservoirs across the dermatomed neonatal porcine skin over 24 h.

Drug	Hydrogel formulation (%w/w in water)	Reservoir type	Drug permeated from 0.5 cm^2 MN arrays	
			(mg)	(%)
RIF	20% Gantrez® S-97, 7.5% PEG 10,000, 3% Na_2CO_3 (H1)	LYO	0.10 ± 0.00	0.14 ± 0.00
		DCT	0.68 ± 0.04	0.65 ± 0.04
		PEG	8.25 ± 0.90	75.06 ± 8.21
INH	15% PVA, 10% PVP, 1.5% citric acid (H3)	LYO	58.45 ± 4.02	79.23 ± 5.46
		DCT	18.95 ± 1.23	13.30 ± 0.86
		PEG	9.21 ± 0.87	83.75 ± 7.98
PYR	15% PVA, 10% PVP, 1.5% citric acid (H3)	LYO	20.08 ± 0.73	20.08 ± 0.73
		DCT	16.71 ± 0.72	13.11 ± 0.57
		PEG	8.81 ± 1.39	80.12 ± 12.66
ETH	20% Gantrez® S-97, 7.5% PEG 10,000, 3% Na_2CO_3 (H1)	LYO	17.01 ± 1.84	22.68 ± 2.46
		DCT	46.99 ± 5.81	46.99 ± 5.81
		PEG	8.25 ± 0.90	75.06 ± 8.21

formulation. This result was in good agreement with the FTIR analysis, as may be attributed to the completed drug dispersion into the mixture of PEG 200 and PEG 6,000.

3.11. *In vitro permeation studies*

In vitro permeation studies were conducted in order to determine the permeation profile of each drug across the dermatomed 350 μm neonatal porcine skin. Several studies have been performed using this *in vitro* method to investigate the delivery of ibuprofen-sodium, ovalbumin, metformin, donepezil HCl and olanzapine [18,23,25,41]. In this work, three types of reservoirs for each drug were compared to investigate the versatility of hydrogel-forming MN arrays delivering drugs from designated reservoirs. A drug reservoir was incorporated with a specific hydrogel-forming MN array formulation such as Gantrez® S-97-based MN array (H1) for RIF and ETH, whilst the PVA-based formulation (H3) was used for INH and PYR. Results of cumulative drug permeation in 24 h are displayed in Fig. 12 and Table 8.

In the case of RIF, approximately 3.64 mg could be delivered from the PEG solid reservoir incorporated with Gantrez® S-97-based formulation (H1) across the dermatomed porcine skin in 24 h. This result is clearly associated with high molecular weight and hydrophobicity which could have led to low permeation through hydrogel-forming MN arrays prepared from Gantrez® S-97. However, this delivered concentration was significantly higher compared to the permeation results from LYO and DCT reservoir ($p < 0.05$). By utilising solid dispersion technique, PEG could increase RIF solubility due to its aqueous miscibility [77]. When the reservoir was incorporated on the MN array and it attached to the skin, hydrogel system can provide an aqueous environment by imbibing interstitial fluid from lower dermal layers of the skin. By dissolving RIF in PEG matrix which has both hydrophilic and hydrophobic characteristics, this can allow the hydrophobic drug molecules to permeate through an aqueous network of swollen MN arrays. Moreover, lower permeation of RIF from LYO reservoir could be explained by the RIF aggregation. This could possibly resulting in difficulties of liquid imbibed in hydrogel-forming MN arrays to disintegrate and dissolve the LYO, as RIF particles, which are insoluble, covered the surface of the reservoir in contact with the MN array base [78].

ETH permeation was significantly higher from DCT reservoirs compared to LYO and PEG reservoirs using Gantrez® S-97-based MN arrays (H1) ($p < 0.05$). The combination of DCT reservoir with Gantrez® S-97-based MN arrays had successfully delivered ETH about a three-fold in 24 h higher than that delivered from LYO reservoirs. It is notable that ETH experienced a lag time to then achieve a burst release at 8 h followed by a slight increment at 24 h, possibly due to the absence of disintegrant in the DCT reservoirs.

Following the application of drug reservoir with the prepared PVA-based MN arrays (H3) on the dermatomed porcine skin for 24 h, a similar trend was observed from the permeation profiles of INH and PYR. The drug amount permeated from LYO reservoir was significantly higher than DCTs and PEG solid reservoirs ($p < 0.05$). LYO reservoirs have a hygroscopic characteristic due to the porous structure formed during the drying process. This property might increase the reservoir solubility [79–81]. Contrastingly, an inferior permeation is possibly related to the greater volume of fluid that is required to disintegrate and dissolve the DCT reservoir, due to its higher compaction. Thus, a lower amount of drug was allowed to permeate through the MN arrays and the neonatal porcine skin. Moreover, a lower amount of drug could be loaded into the PEG solid reservoir, accordingly it may be related with the low amount of delivered drug through the hydrogel-forming MN arrays.

Based on the data provided in Table 8, the most promising reservoirs for RIF, INH, PYR and ETH were PEG, LYO, LYO, DCT, respectively.

Regarding the proposed patch size, this can be extrapolated using the *in vitro* permeation data (Table 8) considering oral bioavailability. The oral bioavailability was selected due to the lack of available data for transdermal pharmacokinetic of TB drugs. Fixed-dose combination of TB drugs consists of RIF (150 mg), INH (75 mg), PYR (400 mg) and ETH (275 mg) with an oral bioavailability of 68%, ~100%, 90% and 80%, respectively [82]. Accordingly, the drug doses that have to be effectively delivered for RIF, INH, PYR and ETH are 102 mg, 75 mg, 360 mg and 220 mg, respectively. Therefore, correlating our *in vitro* permeation data with oral bioavailability, we can estimate the patch sizes for daily human adult treatment as 6.18 cm^2, 0.63 cm^2, 8.96 cm^2 and 2.34 cm^2 for RIF, INH, PYR and ETH, respectively. These patch sizes are considered acceptable for clinical human application due to the design of MN arrays required is <10 cm^2 [83].

Overall, the results of the present work have described the versatility of hydrogel-forming MN arrays to deliver different TB drugs across the skin, using different types of drug reservoirs. Specifically, the drugs investigated in this study varied in terms of hydrophobicity and chemical structures. For the first time, we have successfully efficiently delivered these drugs across the skin by selecting one of two hydrogel-forming MN arrays coupled with one of three drug reservoirs. This approach might be used as a preliminary step to design hydrogel-forming MN system for the delivery of high-dose drugs with different molecular properties. In the future, solubility and physicochemical properties of drugs will be used as factors to determine reservoir design and hydrogel composition. In comparison to a regular transdermal patch that can deliver only approximately 10% of the loaded active compound [14], this system was able to deliver up to 85% of the drug contained in the reservoirs. However, *in vivo* pharmacokinetic studies will be required in order to investigate if plasma concentration of drugs are clinically relevant and also, estimate actual patch sizes. Additionally, *in vivo* pharmacodynamic studies also must be performed to evaluate the therapeutic efficacy of this approach in animal models of TB disease.

4. Conclusion

This work presents a successful development of hydrogel-forming MN system, for the first time, to transdermally deliver RIF, INH, PYR and ETH for potential TB treatment. Several formulations of hydrogel films were assessed in terms of swelling capability and solute permeability. Drug reservoirs were formulated using several techniques

including lyophilised, directly compressed and SD of PEG matrix. Subsequently, drug reservoirs were optimised for further *in vitro* studies application. Essentially, the detailed results of *in vitro* permeation studies showed that hydrogel-forming MN arrays could successfully deliver RIF, INH, PYR and ETH from their reservoir across neonate porcine skin. Accordingly, due to its versatility, the result of this study can be considered as a model for developing a wide range of high-dose drugs using hydrogel-forming MN arrays in transdermal delivery purpose. Moreover, the development of this transdermal TB drug regime is still in the early stage, thus a further investigation to evaluate the effectivity, stability, safety, and efficacy prior to the clinical application will be required. For instance, *in vivo* pharmacokinetic studies must be done to determine the plasma concentration of the drug in the animal model. Besides, to ensure the efficacy of this system, pharmacodynamic studies must be also performed. On this basis, to reach clinical practice and ensure the benefit for TB treatment application, this novel approach should be tested in terms of the usability and acceptability to achieve the maximum impact of this work.

Acknowledgement

Authors thank Luki Ahmadi Hari Wardoyo for his support in providing and designing the illustrations included in this manuscript. Authors also gratefully acknowledge the Indonesian Endowment Fund for Education (Lembaga Pengelola Dana Pendidikan/LPDP) scholarship and the Welcome Trust [WT094085MA] for their financial support to this work.

Appendix A. Supplementary material

Supplementary data to this article can be found online at https://doi.org/10.1016/j.ejpb.2020.12.003.

References

[1] M. Pai, M.A. Behr, D. Dowdy, K. Dheda, M. Divangahi, C.C. Boehme, A. Ginsberg, S. Swaminathan, M. Spigelman, H. Getahun, D. Menzies, M. Raviglione, Tuberculosis, Nat. Rev. Dis. Prim. 2 (2016) 1–23, https://doi.org/10.1038/nrdp.2016.76.

[2] WHO, Global tuberculosis report, World Heal. Organ, 2019.

[3] J. Furin, H. Cox, M. Pai, Tuberculosis, Lancet 393 (2019) 1642–1656, https://doi.org/10.1016/S0140-6736(19)30308-3.

[4] J.G. Douglas, M.J. McLeod, Pharmacokinetic factors in the modern drug treatment of tuberculosis, Clin. Pharmacokinet. 37 (1999) 127–146, https://doi.org/10.2165/00003088-199937020-00003.

[5] S. Ahmad, E. Mokaddas, Current status and future trends in the diagnosis and treatment of drug-susceptible and multidrug-resistant tuberculosis, J. Infect. Public Health. 7 (2014) 75–91, https://doi.org/10.1016/j.jiph.2013.09.001.

[6] A. Zumla, J. Chakaya, R. Centis, L. D'Ambrosio, P. Mwaba, M. Bates, N. Kapata, T. Nyirenda, D. Chanda, S. Mfinanga, M. Hoelscher, M. Maeurer, G.B. Migliori, Tuberculosis treatment and management-an update on treatment regimens, trials, new drugs, and adjunct therapies, Lancet Respir. Med. 3 (2015) 220–234, https://doi.org/10.1016/S2213-2600(15)00063-6.

[7] D.D. Pham, E. Fattal, N. Tsapis, Pulmonary drug delivery systems for tuberculosis treatment, Int. J. Pharm. 478 (2015) 517–529, https://doi.org/10.1016/j.ijpharm.2014.12.009.

[8] N. Litaiem, S. Youssef, K. Jabeur, M.R. Dhaoui, N. Doss, Affective temperament profile in psoriasis patients in Tunisia using TEMPS-A, J. Affect. Disord. 151 (2013) 321–324, https://doi.org/10.1016/j.jad.2013.05.099.

[9] M.M. Mehanna, S.M. Mohyeldin, N.A. Elgindy, Respirable nanocarriers as a promising strategy for antitubercular drug delivery, J. Control. Release. 187 (2014) 183–197, https://doi.org/10.1016/j.jconrel.2014.05.038.

[10] L.C. du Toit, V. Pillay, M.P. Danckwerts, Tuberculosis chemotherapy: Current drug delivery approaches, Respir. Res. 7 (2006) 118, https://doi.org/10.1186/1465-9921-7-118.

[11] D. Prabakaran, P. Singh, K.S. Jaganathan, S.P. Vyas, Osmotically regulated asymmetric capsular systems for simultaneous sustained delivery of anti-tubercular drugs, J. Control. Release. 95 (2004) 239–248, https://doi.org/10.1016/j.jconrel.2003.11.013.

[12] D.A. Mitchison, P.B. Fourie, The near future: Improving the activity of rifamycins and pyrazinamide, Tuberculosis. 90 (2010) 177–181, https://doi.org/10.1016/j.tube.2010.03.005.

[13] M.R. Prausnitz, R. Langer, Transdermal drug delivery, Nat. Biotechnol. 26 (2008) 1261–1268, https://doi.org/10.1038/nbt.1504.

[14] K.S. Paudel, M. Milewski, C.L. Swadley, N.K. Brogden, P. Ghosh, A.L. Stinchcomb, Challenges and opportunities in dermal/transdermal delivery, Ther. Deliv. 1 (2010) 109–131, https://doi.org/10.4155/tde.10.16.

[15] R.F. Donnelly, M.J. Garland, D.I.J. Morrow, K. Migalska, R.R.S. Thakur, R. Majithiya, A.D. Woolfson, Optical coherence tomography is a valuable tool in the study of the effects of microneedle geometry on skin penetration characteristics and in-skin dissolution, J. Control. Release. 147 (2010) 333–341, https://doi.org/10.1016/j.jconrel.2010.08.008.

[16] S. Hirobe, H. Azukizawa, K. Matsuo, Y. Zhai, Y.S. Quan, F. Kamiyama, H. Suzuki, I. Katayama, N. Okada, S. Nakagawa, Development and clinical study of a self-dissolving microneedle patch for transcutaneous immunization device, Pharm. Res. 30 (2013) 2664–2674, https://doi.org/10.1007/s11095-013-1092-6.

[17] B. Cai, W. Xia, S. Bredenberg, H. Li, H. Engqvist, Bioceramic microneedles with flexible and self-swelling substrate, Eur. J. Pharm. Biopharm. 94 (2015) 404–410, https://doi.org/10.1016/j.ejpb.2015.06.016.

[18] R.F. Donnelly, M.T.C. McCrudden, A.Z. Alkilani, E. Larrañeta, E. McAlister, A. J. Courtenay, M.C. Kearney, R.R.S. Thakur, H.O. McCarthy, V.L. Kett, E. Caffarel-Salvador, S. Al-Zahrani, A.D. Woolfson, Hydrogel-forming microneedles prepared from "super swelling" polymers combined with lyophilised wafers for transdermal drug delivery, PLoS One 9 (2014) 1–12, https://doi.org/10.1371/journal.pone.0111547.

[19] R.F. Donnelly, K. Moffatt, A.Z. Alkilani, E.M. Vicente-Pérez, J. Barry, M.T. C. McCrudden, A.D. Woolfson, Hydrogel-forming microneedle arrays can be effectively inserted in skin by self-application: A pilot study centred on pharmacist intervention and a patient information leaflet, Pharm. Res. 31 (2014) 1989–1999, https://doi.org/10.1007/s11095-014-1301-y.

[20] R.F. Donnelly, R.R.S. Thakur, A.Z. Alkilani, M.T.C. McCrudden, S. O'Neill, C. O'Mahony, K. Armstrong, N. McLoone, P. Kole, A.D. Woolfson, Hydrogel-forming microneedle arrays exhibit antimicrobial properties: Potential for enhanced patient safety, Int. J. Pharm. 451 (2013) 76–91, https://doi.org/10.1016/j.ijpharm.2013.04.045.

[21] R.F. Donnelly, R.R.S. Thakur, M.J. Garland, K. Migalska, R. Majithiya, C. M. McCrudden, P.L. Kole, T.M.T. Mahmood, H.O. McCarthy, A.D. Woolfson, Hydrogel-forming microneedle arrays for enhanced transdermal drug delivery, Adv. Funct. Mater. 22 (2012) 4879–4890, https://doi.org/10.1002/adfm.201200864.

[22] R.F. Donnelly, R.R.S. Thakur, D.I.J. Morrow, A.D. Woolfson, Microneedle-mediated transdermal and intradermal drug delivery, 2012. doi: 10.1002/9781119959687.

[23] E.M. Migdadi, A.J. Courtenay, I.A. Tekko, M.T.C. McCrudden, M.C. Kearney, E. McAlister, H.O. McCarthy, R.F. Donnelly, Hydrogel-forming microneedles enhance transdermal delivery of metformin hydrochloride, J. Control. Release. 285 (2018) 142–151, https://doi.org/10.1016/j.jconrel.2018.07.009.

[24] X. Gao, N.K. Brogden, Development of hydrogels for microneedle-assisted transdermal delivery of naloxone for opioid-induced pruritus, J. Pharm. Sci. 108 (2019) 3695–3703, https://doi.org/10.1016/j.xphs.2019.08.025.

[25] M.C. Kearney, P.E. McKenna, H.L. Quinn, A.J. Courtenay, E. Larrañeta, R. F. Donnelly, Design and development of liquid drug reservoirs for microneedle delivery of poorly soluble drug molecules, Pharmaceutics. 11 (2019) 1–17, https://doi.org/10.3390/pharmaceutics11110605.

[26] F. AlHusban, Y. Perrie, A.R. Mohammed, Formulation and characterisation of lyophilised rapid disintegrating tablets using amino acids as matrix forming agents, Eur. J. Pharm. Biopharm. 75 (2010) 254–262, https://doi.org/10.1016/j.ejpb.2010.03.012.

[27] R. Laitinen, E. Suihko, M. Bjorkqvist, J. Riikonen, V.P. Lehto, K. Jarvinen, J. Ketolainen, Perphenazine solid dispersions for orally fast-disintegrating tablets: Physical stability and formulation, Drug Dev. Ind. Pharm. 36 (2010) 601–613, https://doi.org/10.3109/03639040903386690.

[28] J. Domínguez-Robles, S.A. Stewart, A. Rendl, Z. González, R.F. Donnelly, E. Larrañeta, Lignin and cellulose blends as pharmaceutical excipient for tablet manufacturing via direct compression, Biomolecules. 9 (2019) 1–17, https://doi.org/10.3390/biom9090423.

[29] I.A. Tekko, G. Chen, J.D. Robles, R.R.S. Thakur, I. Hamdan, L.K. Vora, E. Larrañeta, J.C. McElnay, H.O. McCarthy, M. Rooney, R.F. Donnelly, Development and characterisation of novel poly (vinyl alcohol)/poly (vinyl pyrrolidone)-based hydrogel-forming microneedle arrays for enhanced and sustained transdermal delivery of methotrexate, Int. J. Pharm. 586 (2020) 1–17, https://doi.org/10.1016/j.ijpharm.2020.119580.

[30] R.R.S. Thakur, P.A. McCarron, A.D. Woolfson, R.F. Donnelly, Investigation of swelling and network parameters of poly(ethylene glycol)-crosslinked poly(methyl vinyl ether-co-maleic acid) hydrogels, Eur. Polym. J. 45 (2009) 1239–1249, https://doi.org/10.1016/j.eurpolymj.2008.12.019.

[31] C. Birck, S. Degoutin, N. Tabary, V. Miri, M. Bacquet, New crosslinked cast films based on poly(vinyl alcohol): Preparation and physico-chemical properties, Express Polym. Lett. (2014), https://doi.org/10.3144/expresspolymlett.2014.95.

[32] Y.B. Truong, J. Choi, J. Mardel, Y. Gao, S. Maisch, M. Musameh, I.L. Kyratzis, Functional cross-linked electrospun polyvinyl alcohol membranes and their potential applications, Macromol. Mater. Eng. 302 (2017) 1–9, https://doi.org/10.1002/mame.201700024.

[33] J. Wang, W. Wu, Swelling behaviors, tensile properties and thermodynamic studies of water sorption of 2-hydroxyethyl methacrylate/epoxy methacrylate copolymeric hydrogels, Eur. Polym. J. 41 (2005) 1143–1151, https://doi.org/10.1016/j.eurpolymj.2004.11.034.

[34] H. Omidian, S.A. Hashemi, F. Askari, S. Nafisi, Swelling and crosslink density measurements for hydrogels, Iran. J. Polym. Sci. Technol. 3 (1994) 115–119.

[35] R.S.H. Wong, M. Ashton, K. Dodou, Effect of crosslinking agent concentration on the properties of unmedicated hydrogels, Pharmaceutics. 7 (2015) 305–319, https://doi.org/10.3390/pharmaceutics7030305.
[36] B.J. Tighe, Role of permeability and related properties in the design of synthetic hydrogels for biomedical applications, Br. Polym. J. 18 (1986) 8–13, https://doi.org/10.1002/pi.4980180104.
[37] R.F. Donnelly, D.I.J. Morrow, M.T.C. McCrudden, A.Z. Alkilani, E.M. Vicente-Pérez, C. O'Mahony, P. González-Vázquez, P.A. McCarron, A.D. Woolfson, Hydrogel-forming and dissolving microneedles for enhanced delivery of photosensitizers and precursors, Photochem. Photobiol. 90 (2014) 641–647, https://doi.org/10.1111/php.12209.
[38] E. Larrañeta, J. Moore, E.M. Vicente-Pérez, P. González-Vázquez, R. Lutton, A. D. Woolfson, R.F. Donnelly, A proposed model membrane and test method for microneedle insertion studies, Int. J. Pharm. 472 (2014) 65–73, https://doi.org/10.1016/j.ijpharm.2014.05.042.
[39] H. Van Ngo, V.T.K. Ngo, V.T. Vo, P.K. Nguyen, T. Vo Van, P.H.L. Tran, T.T.D. Tran, Effects of absorbent on the dissolution rate of PEG-based solid dispersions containing poorly water-soluble drug, in: IFMBE Proc., 2018, pp. 515–518. doi: 10.1007/978-981-10-4361-1_87.
[40] A.T.M. Serajuddln, Solid dispersion of poorly water-soluble drugs: Early promises, subsequent problems, and recent breakthroughs, J. Pharm. Sci. 88 (1999) 1058–1066, https://doi.org/10.1021/js980403l.
[41] M.C. Kearney, E. Caffarel-Salvador, S.J. Fallows, H.O. McCarthy, R.F. Donnelly, Microneedle-mediated delivery of donepezil: Potential for improved treatment options in Alzheimer's disease, Eur. J. Pharm. Biopharm. 103 (2016) 43–50, https://doi.org/10.1016/j.ejpb.2016.03.026.
[42] N. Kashyap, N. Kumar, M.N.V.R. Kumar, Hydrogels for pharmaceutical and biomedical applications, Crit. Rev. Ther. Drug Carrier Syst. 22 (2005) 107–149, https://doi.org/10.1615/CritRevTherDrugCarrierSyst.v22.i2.10.
[43] N.A. Peppas, P. Bures, W. Leobandung, H. Ichikawa, Hydrogels in pharmaceutical formulations, Eur. J. Pharm. Biopharm. 50 (2000) 27–46, https://doi.org/10.1016/S0939-6411(00)00090-4.
[44] S.H. Khalid, M.I. Qadir, A. Massud, M. Ali, M.H. Rasool, Effect of degree of cross-linking on swelling and drug release behaviour of poly(methyl methacrylate-co-itaconic acid) [P(MMA/IA)] hydrogels for site specific drug delivery, J. Drug Deliv. Sci. Technol. 19 (2009) 413–418, https://doi.org/10.1016/S1773-2247(09)50085-8.
[45] J. Ostrowska-Czubenko, M. Gierszewska, M. Pieróg, pH-responsive hydrogel membranes based on modified chitosan: Water transport and kinetics of swelling, J. Polym. Res. 22 (2015) 1–12, https://doi.org/10.1007/s10965-015-0786-3.
[46] A.R. Khare, N.A. Peppas, Swelling/deswelling of anionic copolymer gels, Biomaterials 16 (1995) 559–567, https://doi.org/10.1016/0142-9612(95)91130-Q.
[47] L. Yu, L. Gu, Hydrolyzed polyacrylonitrile-blend-soy protein hydrogel fibers: A study of structure and dynamic pH response, Polym. Int. 58 (2009) 66–73, https://doi.org/10.1002/pi.2493.
[48] S.H. Gehrke, J.P. Fisher, M. Palasis, M.E. Lund, Factors determining hydrogel permeability, Ann. N. Y. Acad. Sci. 831 (1997) 179–207, https://doi.org/10.1111/j.1749-6632.1997.tb52194.x.
[49] A.R.C. Duarte, A.S.D. Ferreira, S. Barreiros, E. Cabrita, R.L. Reis, A. Paiva, A comparison between pure active pharmaceutical ingredients and therapeutic deep eutectic solvents: Solubility and permeability studies, Eur. J. Pharm. Biopharm. 114 (2017) 296–304, https://doi.org/10.1016/j.ejpb.2017.02.003.
[50] R. Zhang, M. Tang, A. Bowyer, R. Eisenthal, J. Hubble, A novel pH- and ionic-strength-sensitive carboxy methyl dextran hydrogel, Biomaterials 26 (2005) 4677–4683, https://doi.org/10.1016/j.biomaterials.2004.11.048.
[51] R.M. Ottenbrite, K. Park, T. Okano, Biomedical Applications of Hydrogels Handbook, Springer Science+Business Media, LLC, 2010. doi: 10.1007/978-1-4419-5919-5.
[52] E. Larrañeta, S. Stewart, M. Ervine, R. Al-Kasasbeh, R.F. Donnelly, Hydrogels for hydrophobic drug delivery: Classification, synthesis and applications, J. Funct. Biomater. 9 (2018) 1–20, https://doi.org/10.3390/jfb9010013.
[53] J. Li, D.J. Mooney, Designing hydrogels for controlled drug delivery, Nat. Rev. Mater. 1 (2016) 1–17, https://doi.org/10.1038/natrevmats.2016.71.
[54] A.D. Permana, I.A. Tekko, M.T.C. McCrudden, Q.K. Anjani, D. Ramadon, H. O. McCarthy, R.F. Donnelly, Solid lipid nanoparticle-based dissolving microneedles: A promising intradermal lymph targeting drug delivery system with potential for enhanced treatment of lymphatic filariasis, J. Control. Release. 316 (2019) 34–52, https://doi.org/10.1016/j.jconrel.2019.10.004.
[55] P. González-Vázquez, E. Larrañeta, M.T.C. McCrudden, C. Jarrahian, A. Rein-Weston, M. Quintanar-Solares, D. Zehrung, H. McCarthy, A.J. Courtenay, R. F. Donnelly, Transdermal delivery of gentamicin using dissolving microneedle arrays for potential treatment of neonatal sepsis, J. Control. Release. 265 (2017) 30–40, https://doi.org/10.1016/j.jconrel.2017.07.032.
[56] M.T.C. McCrudden, E. Larrañeta, A. Clark, C. Jarrahian, A. Rein-Weston, S. Lachau-Durand, N. Niemeijer, P. Williams, C. Haeck, H.O. McCarthy, D. Zehrung, R. F. Donnelly, Design, formulation and evaluation of novel dissolving microarray patches containing a long-acting rilpivirine nanosuspension, J. Control. Release. 292 (2018) 119–129, https://doi.org/10.1016/j.jconrel.2018.11.002.
[57] M.G. Fakes, M.V. Dali, T.A. Haby, K.R. Morris, S.A. Varia, A.T.M. Serajuddin, Moisture sorption behavior of selected bulking used in lyophilized products, PDA J. Pharm. Sci. Technol. 54 (2000) 144–149.
[58] D.B. Varshney, S. Kumar, E.Y. Shalaev, P. Sundaramurthi, S.W. Kang, L.A. Gatlin, R. Suryanarayanan, Glycine crystallization in frozen and freeze-dried systems: Effect of pH and buffer concentration, Pharm. Res. 24 (2007) 593–604, https://doi.org/10.1007/s11095-006-9178-z.
[59] M.J. Akers, Sterilization Methods in Sterile Product Manufacturing, Informa Healthcare, New York, 2010.
[60] D. Novakovic, A. Isomäki, B. Pleunis, S.J. Fraser-Miller, L. Peltonen, T. Laaksonen, C.J. Strachan, Understanding dissolution and crystallization with imaging: A surface point of view, Mol. Pharm. 15 (2018) 5361–5373, https://doi.org/10.1021/acs.molpharmaceut.8b00840.
[61] K.A. Gaidhani, M. Harwalkar, D. Bhambere, P.S. Nirgude, Lyophilization/freeze drying: A review, World J. Pharm. Res. 4 (2015) 516–543.
[62] G.H.E. Meister, A significant comparison between collapse and glass transition temperatures, Eur. Pharm. Rev. (2008). https://www.europeanpharmaceuticalreview.com/article/1479/a-significant-comparison-between-collapse-and-glass-transition-temperatures/ (accessed March 11, 2020).
[63] B.S. Chang, C.S. Randall, Use of subambient thermal analysis to optimize protein lyophilization, Cryobiology 29 (1992) 632–656, https://doi.org/10.1016/0011-2240(92)90067-C.
[64] A.P. MacKenzie, The physico-chemical basis for the freeze-drying process, Dev. Biol. Stand. 36 (1977) 51–67.
[65] F. Franks, Freeze-drying: from empiricism to predictability. The significance of glass transitions, Dev. Biol. Stand. 11 (1992) 93–110.
[66] L.M. Her, S.L. Nail, Measurement of glass transition temperatures of freeze-concentrated solutes by differential scanning calorimetry, Pharm. Res. An Off. J. Am. Assoc. Pharm. Sci. 11 (1994) 54–59, https://doi.org/10.1023/A:1018989509893.
[67] E.Y. Shalaev, A.N. Kanev, Study of the solid-liquid state diagram of the water-glycine-sucrose system, Cryobiology 31 (1994) 374–382, https://doi.org/10.1006/cryo.1994.1045.
[68] A. Baheti, L. Kumar, A.K. Bansal, Excipients used in lyophilization of small molecules, J. Excipients Food Chem. 1 (2010) 41–54.
[69] R. Alves, T.V.D.S. Reis, L.C.C. Da Silva, S. Storpírtis, L.P. Mercuri, J.D.R. Matos, Thermal behavior and decomposition kinetics of rifampicin polymorphs under isothermal and non-isothermal conditions, Brazilian J. Pharm. Sci. 46 (2010) 343–351, https://doi.org/10.1590/S1984-82502010000200022.
[70] J.M. Rubin-Preminger, J. Bernstein, R.K. Harris, I.R. Evans, P.Y. Ghi, Variable temperature studies of a polymorphic system comprising two pairs of enantiotropically related forms: [S, S]-ethambutol dihydrochloride, Cryst. Growth Des. 4 (2004) 431–439, https://doi.org/10.1021/cg0341959.
[71] S. Ohtake, Y. Kita, T. Arakawa, Interactions of formulation excipients with proteins in solution and in the dried state, Adv. Drug Deliv. Rev. 63 (2011) 1053–1073, https://doi.org/10.1016/j.addr.2011.06.011.
[72] L.L. Augsburger, S.W. Hoag, Pharmaceutical dosage forms: Capsules, 2017. doi: 10.1201/b19825.
[73] S. Chono, K. Nakamura, M. Matsui, Physical properties of lansoprazole orally disintegrating tablets, J. Generic Med. 13 (2017) 5–8, https://doi.org/10.1177/1741134316673226.
[74] N.K. Thakral, S. Mohapatra, G.A. Stephenson, R. Suryanarayanan, Compression-induced crystallization of amorphous indomethacin in tablets: Characterization of spatial heterogeneity by two-dimensional X-ray diffractometry, Mol. Pharm. 12 (2015) 253–263, https://doi.org/10.1021/mp5005788.
[75] S. Afifi, Solid dispersion approach improving dissolution rate of stiripentol: A novel antiepileptic drug, Iran. J. Pharm. Res. 14 (2015) 1001–1014, https://doi.org/10.22037/ijpr.2015.1725.
[76] H. Larhrib, J.I. Wells, M.H. Rubinstein, Compressing polyethylene glycols: The effect of compression pressure and speed, Int. J. Pharm. 147 (1997) 199–205, https://doi.org/10.1016/S0378-5173(96)04818-1.
[77] N. Bolourchian, M.M. Mahboobian, S. Dadashzadeh, The effect of PEG molecular weights on dissolution behavior of simvastatin in solid dispersions, Iran. J. Pharm. Res. 12 (2013) 11–20, https://doi.org/10.22037/ijpr.2013.1267.
[78] E. Grotz, E. Bernabeu, M. Pappalardo, D.A. Chiappetta, M.A. Moretton, Nanoscale Kolliphor® HS 15 micelles to minimize rifampicin self-aggregation in aqueous media, J. Drug Deliv. Sci. Technol. 41 (2017) 1–6, https://doi.org/10.1016/j.jddst.2017.06.009.
[79] M. Dixit, A.G. Kini, P.K. Kulkarni, Enhancing the aqueous solubility and dissolution of olanzapine using freeze-drying, Brazilian J. Pharm. Sci. 47 (2011) 743–749, https://doi.org/10.1590/S1984-82502011000400011.
[80] M. Dixit, P.K. Kulkarni, Lyophilization monophase solution technique for improvement of the solubility and dissolution of piroxicam, Res. Pharm. Sci. 7 (2012) 13–21.
[81] P.W. Dhore, V.S. Dave, S.D. Saoji, Y.S. Bobde, C. Mack, N.A. Raut, Enhancement of the aqueous solubility and permeability of a poorly water soluble drug ritonavir via lyophilized milk-based solid dispersions, Pharm. Dev. Technol. 22 (2017) 90–102, https://doi.org/10.1080/10837450.2016.1193193.
[82] L.S. Goodman, A. Gilman, J.G. Hardman, A.G. Gilman, L.E. Limbird, Goodman & Gilman's the pharmacological basis of therapeutics, 12th ed. in: New York McGraw-Hill, Heal. Prof. Div., 2011, pp. 1–35.
[83] M.T.C. McCrudden, A.Z. Alkilani, C.M. McCrudden, E. McAlister, H.O. McCarthy, A.D. Woolfson, R.F. Donnelly, Design and physicochemical characterisation of novel dissolving polymeric microneedle arrays for transdermal delivery of high dose, low molecular weight drugs, J. Control. Release. 180 (2014) 71–80, https://doi.org/10.1016/j.jconrel.2014.02.007.